Structure-Property Relationships of Unsupported Diiridium(II) Complexes with Variation of Axial Ligand

Siye Wu,[a] *Shunan Zhao,*[a] *Fangrui Zheng,**[a,b] *Keith Man-Chung Wong**[a]

[a]Department of Chemistry, Southern University of Science and Technology, No. 1088, Xueyuan Boulevard, Nanshan District, Shenzhen 518055, P.R. China.

E-mail: keithwongmc@sustech.edu.cn

[b]Analysis and Testing Center, Shenzhen Technology University, 3002 Lantian Road, Shenzhen 518118, P. R. China.

E-mail: zhengfangrui@sztu.edu.cn

Supporting information

Table S1 Crystal and structure determination data of **A-I**.

	A-I
Empirical formula	$C_{62}H_{76}F_6I_2Ir_2N_8O_8S_2$
Formula weight	1877.62
Temperature [K]	100.00
Crystal system	triclinic
Space group (number)	*P*-1 (2)
a [Å]	12.6903(16)
b [Å]	13.2412(16)
c [Å]	13.5259(17)
α [°]	82.166(4)
β [°]	62.989(4)
γ [°]	61.730(4)
Volume [Å^3]	1774.4(4)
Z	1
ρ_{calc} [gcm^{-3}]	1.757
μ [mm^{-1}]	10.197
F(000)	914
Crystal size [mm^3]	0.21×0.18×0.1
Crystal colour	orange
Crystal shape	plate
Radiation	GaK_α (λ=1.34139 Å)
2θ range [°]	7.45 to 113.84 (0.80 Å)
Index ranges	$-15 \leq h \leq 15$
	$-16 \leq k \leq 15$
	$-16 \leq l \leq 16$
Reflections collected	23223
Independent reflections	7185
	R_{int} = 0.0582
	R_{sigma} = 0.0569
Completeness to θ = 53.594°	99.8 %
Data / Restraints / Parameters	7185/6/447
Goodness-of-fit on F^2	1.104
Final *R* indexes [$I \geq 2\sigma(I)$]	R_1 = 0.0414, wR_2 = 0.1267
Final *R* indexes [all data]	R_1 = 0.0494, wR_2 = 0.1373
Largest peak/hole [eÅ^{-3}]	1.19/-0.99

[a] $R_{int} = \Sigma \left| F_o^2 - F_o^2 \text{ (mean)} \right| / \Sigma[F_o^2]$, $R_1 = \Sigma||F_o| - |F_c|| / \Sigma||F_o|$ and $wR_2 = \{\square w(F_o^2 - F_c^2)^2] / \square w(F_o^2)^2]\}^{1/2}$.

Table S2 Selected bond lengths (Å) and angles (deg) for **A-I**.

Bond Lengths (Å)		Bond Angles (deg)	
Ir1–Ir1$^{\#1}$	2.7807(5)	I1–Ir1–Ir1$^{\#1}$	179.689(12)
Ir1–I1	2.7426(5)	C1–Ir1–N3	100.58(18)
Ir1–N3	2.053(4)	C1–Ir1–N1	100.83(17)
Ir1–N1	2.058(3)	C1–Ir1–N2	177.32(16)
Ir1–N2	1.994(4)	N3–Ir1–N1	158.02(17)
Ir1–C1	1.888(5)	N2–Ir1–N3	79.18(15)
O1–C1	1.130(6)	N2–Ir1–N1	79.20(15)

Table S3 Crystal and structure determination data of **A-Br**.

	A-Br
Empirical formula	$C_{62}H_{76}Br_2F_6Ir_2N_8O_8S_2$
Formula weight	1783.64
Temperature [K]	100.0
Crystal system	triclinic
Space group (number)	*P*-1 (2)
a [Å]	12.5790(15)
b [Å]	13.1915(17)
c [Å]	13.5422(17)
α [°]	73.079(4)
β [°]	62.705(4)
γ [°]	61.633(4)
Volume [Å^3]	1749.4(4)
Z	1
ρ_{calc} [gcm^{-3}]	1.693
μ [mm^{-1}]	6.465
F(000)	878
Crystal size [mm^3]	0.2×0.15×0.08
Crystal colour	yellow
Crystal shape	plate
Radiation	GaK_α (λ=1.34139 Å)
2θ range [°]	7.78 to 113.92 (0.80 Å)
Index ranges	$-15 \leq h \leq 15$
	$-16 \leq k \leq 16$
	$-16 \leq l \leq 16$
Reflections collected	18009
Independent reflections	7005
	R_{int} = 0.0572
	R_{sigma} = 0.0636
Completeness to θ = 53.594°	99.0 %
Data / Restraints / Parameters	7005/0/446
Goodness-of-fit on F^2	1.072
Final *R* indexes [$I \geq 2\sigma(I)$]	R_1 = 0.0423, wR_2 = 0.1184
Final *R* indexes [all data]	R_1 = 0.0448, wR_2 = 0.1208
Largest peak/hole [eÅ^{-3}]	1.24/−0.91

[a] $R_{int} = \Sigma \left| F_o^2 - F_o^2 \text{ (mean)} \right| / \Sigma[F_o^2]$, $R_1 = \Sigma||F_o| - |F_c|| / \Sigma|F_o|$ and $wR_2 = \{\square w(F_o^2 - F_c^2)^2] / \square w(F_o^2)^2]\}^{1/2}$.

Table S4 Selected bond lengths (Å) and angles (deg) for **A-Br**.

Bond Lengths (Å)		Bond Angles (deg)	
Ir1–Ir1$^{\#1}$	2.7668(4)	Br1–Ir1–Ir1$^{\#1}$	178.874(13)
Ir1–Br1	2.5788(5)	N2–Ir1–N3	79.45(14)
Ir1–N2	1.987(3)	N2–Ir1–N1	79.23(14)
Ir1–N3	2.051(3)	N3–Ir1–N1	158.28(15)
Ir1–N1	2.052(3)	C1–Ir1–N2	177.47(14)
Ir1–C1	1.877(5)	C1–Ir1–N3	100.60(16)
O1–C1	1.144(6)	C1–Ir1–N1	100.51(16)

Table S5 Crystal and structure determination data of **A-Cl**.

	A-Cl
Empirical formula	$C_{62}H_{77}Cl_2F_6Ir_2N_6O_9S_2$
Formula weight	1683.71
Temperature [K]	99.99
Crystal system	monoclinic
Space group (number)	$P2_1/c$ (14)
a [Å]	13.0945(3)
b [Å]	13.0844(3)
c [Å]	20.9513(5)
α [°]	90
β [°]	93.7000(10)
γ [°]	90
Volume [Å^3]	3582.18(14)
Z	2
ρ_{calc} [gcm^{-3}]	1.561
μ [mm^{-1}]	8.911
F(000)	1674
Crystal size [mm^3]	0.21×0.19×0.17
Crystal colour	yellow
Crystal shape	block
Radiation	CuK_α (λ=1.54178 Å)
2θ range [°]	7.97 to 130.41 (0.85 Å)
Index ranges	$-15 \leq h \leq 15$
	$-15 \leq k \leq 15$
	$-24 \leq l \leq 24$
Reflections collected	73373
Independent reflections	6086
	R_{int} = 0.0388
	R_{sigma} = 0.0174
Completeness to θ = 65.207°	99.3 %
Data / Restraints / Parameters	6086/60/444
Goodness-of-fit on F^2	1.093
Final R indexes [$I \geq 2\sigma(I)$]	R_1 = 0.0374, wR_2 = 0.1061
Final R indexes [all data]	R_1 = 0.0390, wR_2 = 0.1081
Largest peak/hole [eÅ^{-3}]	1.70/−0.45

[a] $R_{int} = \Sigma \left| F_o^2 - F_o^2 \text{ (mean)} \right| / \Sigma[F_o^2]$, $R_1 = \Sigma||F_o| - |F_c|| / \Sigma||F_o|$ and $wR_2 = \{\square w(F_o^2 - F_c^2)^2] / \square w(F_o^2)^2]\}^{1/2}$.

Table S6 Selected bond lengths (Å) and angles (deg) for **A-Cl**.

Bond Lengths (Å)		Bond Angles (deg)	
Ir1–Ir1$^{\#1}$	2.7567(3)	Cl1–Ir1–Ir1$^{\#1}$	177.21(3)
Ir1–Cl1	2.4482(10)	N2–Ir1–N1	79.33(14)
Ir1–N2	1.994(3)	N2–Ir1–N3	79.57(14)
Ir1–N1	2.056(4)	N3–Ir1–N1	158.42(14)
Ir1–N3	2.052(4)	C28–Ir1–N2	177.75(16)
Ir1–C28	1.882(4)	C28–Ir1–N1	101.05(17)
O1–C28	1.136(5)	C28–Ir1–N3	99.87(16)

Table S7 Crystal and structure determination data of **A-SCN**.

	A-SCN
Empirical formula	$C_{60}H_{70}F_6Ir_2N_8O_8S_4$
Formula weight	1657.88
Temperature [K]	100.00
Crystal system	monoclinic
Space group (number)	$P2_1/n$ (14)
a [Å]	14.7806(17)
b [Å]	13.1133(16)
c [Å]	20.145(2)
α [°]	90
β [°]	107.790(4)
γ [°]	90
Volume [Å^3]	3717.9(8)
Z	2
ρ_{calc} [gcm^{-3}]	1.481
μ [mm^{-1}]	5.588
F(000)	1644
Crystal size [mm^3]	0.3×0.06×0.05
Crystal colour	orange
Crystal shape	needle
Radiation	GaK_α (λ=1.34139 Å)
2θ range [°]	7.10 to 114.59 (0.80 Å)
Index ranges	$-18 \leq h \leq 18$
	$-16 \leq k \leq 16$
	$-25 \leq l \leq 25$
Reflections collected	50663
Independent reflections	7593
	R_{int} = 0.0791
	R_{sigma} = 0.0458
Completeness to θ = 53.594°	99.8 %
Data / Restraints / Parameters	7593/0/406
Goodness-of-fit on F^2	1.086
Final R indexes [$I \geq 2\sigma(I)$]	R_1 = 0.0356, wR_2 = 0.1039
Final R indexes [all data]	R_1 = 0.0381, wR_2 = 0.1056
Largest peak/hole [eÅ^{-3}]	1.34/−0.78

[a] $R_{int} = \Sigma \left| F_o^2 - F_o^2 \text{ (mean)} \right| / \Sigma[F_o^2]$, $R_1 = \Sigma||F_o| - |F_c|| \ / \ \Sigma||F_o|$ and $wR_2 = \{\square w(F_o^2 - F_c^2)^2] \ / \ \square w(F_o^2)^2]\}^{1/2}$.

Table S8 Selected bond lengths (Å) and angles (deg) for **A-SCN**.

Bond Lengths (Å)		Bond Angles (deg)	
Ir1–Ir1$^{\#1}$	2.7785(4)	C2–S1–Ir1	102.41(14)
Ir1–S1	2.4598(9)	S1–Ir1–Ir1$^{\#1}$	178.12(2)
Ir1–N3	1.995(3)	N3–Ir1–N4	79.27(11)
Ir1–N4	2.043(3)	N3–Ir1–N2	78.98(11)
Ir1–N2	2.062(3)	N4–Ir1–N2	157.87(12)
Ir1–C1	1.890(4)	C1–Ir1–N3	178.67(13)
O1–C1	1.132(4)	C1–Ir1–N4	100.20(13)
		C1–Ir1–N2	101.45(13)

Table S9 Crystal and structure determination data of **A-PF**.

	A-PF
Empirical formula	$C_{110}H_{115}F_{18}Ir_2N_{13}O_{14}P_2S_4$
Formula weight	2759.72
Temperature [K]	100.0
Crystal system	monoclinic
Space group (number)	$P2_1/n$ (14)
a [Å]	16.4123(10)
b [Å]	14.4943(9)
c [Å]	25.3140(15)
α [°]	90
β [°]	95.993(3)
γ [°]	90
Volume [Å^3]	5988.9(6)
Z	2
ρ_{calc} [gcm^{-3}]	1.530
μ [mm^{-1}]	3.921
F(000)	2776
Crystal size [mm^3]	0.2×0.1×0.02
Crystal colour	orange
Crystal shape	plate
Radiation	GaK_α (λ=1.34139 Å)
2θ range [°]	5.88 to 113.94 (0.80 Å)
Index ranges	$-20 \leq h \leq 18$
	$-18 \leq k \leq 18$
	$-31 \leq l \leq 31$
Reflections collected	55542
Independent reflections	12053
	R_{int} = 0.0599
	R_{sigma} = 0.0422
Completeness to θ = 53.594°	99.1 %
Data / Restraints / Parameters	12053/31/771
Goodness-of-fit on F^2	1.050
Final R indexes [$I \geq 2\sigma(I)$]	R_1 = 0.0356, wR_2 = 0.0961
Final R indexes [all data]	R_1 = 0.0453, wR_2 = 0.1041
Largest peak/hole [eÅ^{-3}]	1.20/−0.71

[a] $R_{int} = \Sigma \left| F_o^2 - F_o^2 \text{ (mean)} \right| / \Sigma[F_o^2]$, $R_1 = \Sigma||F_o| - |F_c|| / \Sigma||F_o|$ and $wR_2 = \{\square w(F_o^2 - F_c^2)^2] / \square w(F_o^2)^2]\}^{1/2}$.

Table S10 Selected bond lengths (Å) and angles (deg) for **A-PF**.

Bond Lengths (Å)		Bond Angles (deg)	
Ir1–Ir1$^{\#1}$	2.9269(3)	P1–Ir1–Ir1$^{\#1}$	178.10(2)
Ir1–P1	2.4352(9)	N2–Ir1–N1	79.29(12)
Ir1–N2	2.002(3)	N2–Ir1–N3	78.64(12)
Ir1–N1	2.073(3)	N1–Ir1–N3	157.90(12)
Ir1–N3	2.080(3)	C28–Ir1–N2	176.82(14)
Ir1–C28	1.894(4)	C28–Ir1–N1	98.60(14)
O1–C28	1.132(4)	C28–Ir1–N3	103.50(14)

Table S11 Crystal and structure determination data of **A-PCl**.

	A-PCl
Empirical formula	$C_{96}H_{94}Cl_6F_{12}Ir_2N_6O_{14}P_2S_4$
Formula weight	2571.05
Temperature [K]	100.0
Crystal system	monoclinic
Space group (number)	$P2_1/c$ (14)
a [Å]	15.085(2)
b [Å]	19.869(3)
c [Å]	20.382(3)
α [°]	90
β [°]	93.006(7)
γ [°]	90
Volume [Å^3]	6100.6(14)
Z	2
ρ_{calc} [gcm^{-3}]	1.400
μ [mm^{-1}]	4.554
F(000)	2564
Crystal size [mm^3]	0.15×0.1×0.08
Crystal colour	orange
Crystal shape	block
Radiation	GaK_α (λ=1.34139 Å)
2θ range [°]	5.41 to 115.05 (0.79 Å)
Index ranges	$-18 \leq h \leq 18$
	$-24 \leq k \leq 24$
	$-25 \leq l \leq 25$
Reflections collected	72664
Independent reflections	12547
	R_{int} = 0.1017
	R_{sigma} = 0.0734
Completeness to θ = 53.594°	99.9 %
Data / Restraints / Parameters	12547/54/730
Goodness-of-fit on F^2	1.060
Final R indexes [$I \geq 2\sigma(I)$]	R_1 = 0.0617, wR_2 = 0.1685
Final R indexes [all data]	R_1 = 0.0857, wR_2 = 0.1829
Largest peak/hole [eÅ^{-3}]	2.39/−1.83

[a] $R_{int} = \Sigma \left| F_o^2 - F_o^2 \text{ (mean)} \right| / \Sigma[F_o^2]$, $R_1 = \Sigma||F_o| - |F_c|| / \Sigma||F_o|$ and $wR_2 = \{\square w(F_o^2 - F_c^2)^2] / \square w(F_o^2)^2]\}^{1/2}$.

Table S12 Selected bond lengths (Å) and angles (deg) for **A-PCl**.

Bond Lengths (Å)		Bond Angles (deg)	
Ir1–Ir1$^{\#1}$	2.9129(6)	P1–Ir1–Ir1$^{\#1}$	178.06(4)
Ir1–P1	2.5009(15)	N2–Ir1–N3	79.1(2)
Ir1–N2	1.997(5)	N2–Ir1–N1	79.2(2)
Ir1–N3	2.069(5)	N3–Ir1–N1	158.1(2)
Ir1–N1	2.070(5)	C28–Ir1–N2	177.0(2)
Ir1–C28	1.890(7)	C28–Ir1–N3	98.8(2)
O1–C28	1.144(8)	C28–Ir1–N1	103.0(2)

Table S13 Crystal and structure determination data of **A-PBr**.

	A-PBr
Empirical formula	$C_{100}H_{100}Br_6F_{12}Ir_2N_8O_{14}P_2S_4$
Formula weight	2919.91
Temperature [K]	103.0
Crystal system	monoclinic
Space group (number)	*C*2/*c* (15)
a [Å]	28.883(2)
b [Å]	19.606(2)
c [Å]	20.8728(17)
α [°]	90
β [°]	101.350(6)
γ [°]	90
Volume [Å^3]	11588.9(18)
Z	4
ρ_{calc} [gcm^{-3}]	1.674
μ [mm^{-1}]	5.773
F(000)	5736
Crystal size [mm^3]	0.16×0.15×0.06
Crystal colour	orange
Crystal shape	plate
Radiation	GaK_α (λ=1.34139 Å)
2θ range [°]	4.77 to 114.37 (0.80 Å)
Index ranges	$-36 \leq h \leq 35$
	$-24 \leq k \leq 24$
	$-25 \leq l \leq 26$
Reflections collected	87013
Independent reflections	11900
	R_{int} = 0.0937
	R_{sigma} = 0.0581
Completeness to θ = 53.594°	100.0 %
Data / Restraints / Parameters	11900/72/708
Goodness-of-fit on F^2	1.059
Final *R* indexes [$I \geq 2\sigma(I)$]	R_1 = 0.0756, wR_2 = 0.1905
Final *R* indexes [all data]	R_1 = 0.0918, wR_2 = 0.1990
Largest peak/hole [eÅ^{-3}]	2.66/−1.97

[a] $R_{int} = \Sigma \left| F_o^2 - F_o^2 \text{ (mean)} \right| / \Sigma[F_o^2]$, $R_1 = \Sigma||F_o| - |F_c|| / \Sigma|F_o|$ and $wR_2 = \{\square w(F_o^2 - F_c^2)^2] / \square w(F_o^2)^2]\}^{1/2}$.

Table S14 Selected bond lengths (Å) and angles (deg) for **A-PBr**.

Bond Lengths (Å)		Bond Angles (deg)	
Ir1–Ir1$^{\#1}$	2.9303(8)	P1–Ir1–Ir1$^{\#1}$	178.65(6)
Ir1–P1	2.443(2)	N2–Ir1–N1	78.9(3)
Ir1–N2	2.026(7)	N2–Ir1–N3	78.6(3)
Ir1–N1	2.085(7)	N1–Ir1–N3	157.5(3)
Ir1–N3	2.084(7)	C1–Ir1–N2	177.5(4)
Ir1–C1	1.905(10)	C1–Ir1–N1	101.3(3)
O1–C1	1.124(12)	C1–Ir1–N3	101.2(3)

Table S15 Crystal and structure determination data of **A-POMe**.

	A-POMe
Empirical formula	$C_{106}H_{122}F_{12}Ir_2N_6O_{21}P_2S_4$
Formula weight	2618.67
Temperature [K]	100.0
Crystal system	monoclinic
Space group (number)	$P2_1/n$ (14)
a [Å]	15.5313(13)
b [Å]	20.7756(19)
c [Å]	19.5645(17)
α [°]	90
β [°]	110.852(4)
γ [°]	90
Volume [Å^3]	5899.4(9)
Z	2
ρ_{calc} [gcm^{-3}]	1.474
μ [mm^{-1}]	4.055
F(000)	2648
Crystal size [mm^3]	0.25×0.23×0.21
Crystal colour	red
Crystal shape	block
Radiation	GaK_α (λ=1.34139 Å)
2θ range [°]	6.46 to 114.17 (0.80 Å)
Index ranges	$-19 \leq h \leq 19$
	$-25 \leq k \leq 26$
	$-23 \leq l \leq 24$
Reflections collected	61689
Independent reflections	12053
	R_{int} = 0.0665
	R_{sigma} = 0.0521
Completeness to θ = 53.594°	99.9 %
Data / Restraints / Parameters	12053/44/757
Goodness-of-fit on F^2	1.055
Final R indexes [$I \geq 2\sigma(I)$]	R_1 = 0.0480, wR_2 = 0.1360
Final R indexes [all data]	R_1 = 0.0572, wR_2 = 0.1413
Largest peak/hole [eÅ^{-3}]	2.37/−2.41

[a] $R_{int} = \Sigma \left| F_o^2 - F_o^2 \text{ (mean)} \right| / \Sigma[F_o^2]$, $R_1 = \Sigma||F_o| - |F_c|| / \Sigma||F_o|$ and $wR_2 = \{\square w(F_o^2 - F_c^2)^2] / \square w(F_o^2)^2]\}^{1/2}$.

Table S16 Selected bond lengths (Å) and angles (deg) for **A-POMe**.

Bond Lengths (Å)		Bond Angles (deg)	
Ir1–Ir1$^{\#1}$	2.9216(4)	P1–Ir1–Ir1$^{\#1}$	177.64(3)
Ir1–P1	2.4369(11)	N2–Ir1–N1	79.20(15)
Ir1–N2	1.994(4)	N2–Ir1–N3	79.34(15)
Ir1–N1	2.050(4)	N1–Ir1–N3	158.52(14)
Ir1–N3	2.081(4)	C1–Ir1–N2	178.26(16)
Ir1–C1	1.899(5)	C1–Ir1–N1	100.84(17)
O1–C1	1.121(5)	C1–Ir1–N3	100.64(17)

Table S17 The Wiberg bond index of **A-I**, **A-Cl**, **A-SCN** and **A-POMe** in acetonitrile solvent by the SMD B3LYP//B3LYP method.

	Ir-Ir bond (Å) in X-ray	Wiberg
A-I	2.7807(5)	0.86
A-Cl	2.7567(3)	0.91
A-SCN	2.7785(4)	0.86
A-POMe	2.9216(4)	0.74

Table S18 The HOMO–LUMO energy levels and gap values of**A-I**, **A-Cl**, **A-SCN** and **A-POMe** in acetonitrile solvent by the SMD B3LYP//B3LYP method.

	MO	Energy, eV	HOMO-LUMO gap
A-I	Acceptor (LUMO)	-5.478	-3.077
	Donor (HOMO)	-2.402	
A-Cl	Acceptor (LUMO)	-5.717	-3.222
	Donor (HOMO)	-2.495	
A-SCN	Acceptor (LUMO)	-5.583	-3.101
	Donor (HOMO)	-2.482	
A-POMe	Acceptor (LUMO)	-5.007	-2.641
	Donor (HOMO)	-2.366	

Table S19 The key absorption calculations from **A-I** in acetonitrile solvent by the CPCM TD-B3LYP-D3//B3LYP-D3BJ method based on the B3LYP-D3BJ optimized geometries using ORCA 6.0.0. States with fosc (oscillation strength) > 0.01 are shown only. The orbitals with contribution > 0.05 are shown only in the state.

State	Wavelength (nm)	fosc (au**2)	Orbitals (contribution>0.05) †	Transition
4	445	0.053	**434a (HOMO)** -> 436a (0.96)	MMLCT
5	426	0.010	431a -> 435a **(LUMO)** (0.12) 433a -> 436a (0.80)	LLCT+MMLCT
8	305	0.032	**434a (HOMO)** -> 437a (0.28) **434a (HOMO)** -> 438a (0.69)	MMLCT
exp	355/455			

† The corresponding orbitals can be visualized in Figure S51.

Table S20 The key absorption calculations from **A-Cl** in acetonitrile solvent by the CPCM TD-B3LYP-D3//B3LYP-D3BJ method based on the B3LYP-D3BJ optimized geometries using ORCA 6.0.0. States with fosc (oscillation strength) > 0.01 are shown only. The orbitals with contribution > 0.05 are shown only in the state.

State	Wavelength (nm)	fosc (au**2)	Orbitals (contribution>0.05)	Transition
2	421	0.014	397a -> **400a (LUMO+1)** (0.06) **398a (HOMO)** -> **400a (LUMO+1)** (0.89)	MMLCT
5	402	0.057	397a -> **400a (LUMO+1)** (0.90) **398a (HOMO)** -> **400a (LUMO+1)** (0.08)	MMLCT
6	375	0.088	**398a (HOMO)** -> 401a (0.94)	MMLCT
8	367	0.026	397a -> 401a (0.95)	MMLCT
exp	338/413			

† The corresponding orbitals can be visualized in Figure S52.

Table S21 The key absorption calculations from **A-SCN** in acetonitrile solvent by the CPCM TD-B3LYP-D3//B3LYP-D3BJ method based on the B3LYP-D3BJ optimized geometries using ORCA 6.0.0. States with fosc (oscillation strength) > 0.01 are shown only. The orbitals with contribution > 0.05 are shown only in the state.

State	Wavelength (nm)	fosc (au**2)	Orbitals (contribution>0.05)	Transition
2	443	0.046	409a -> **412a (LUMO+1)** (0.23) 409a -> 415a (0.16) **410a (HOMO)** -> **412a (LUMO+1)** (0.55)	MMLCT
3	433	0.055	409a -> **412a (LUMO+1)** (0.20) 409a -> 415a (0.27) **410a (HOMO)** -> **412a (LUMO+1)** (0.42)	MMLCT
6	396	0.049	**410a (HOMO)** -> 413a (0.95)	MMLCT
10	377	0.077	409a -> 413a (0.88)	MMLCT
exp	334/440			

† The corresponding orbitals can be visualized in Figure S53.

Table S22 The key absorption calculations from **A-POMe** in acetonitrile solvent by the CPCM TD-B3LYP-D3//B3LYP-D3BJ method based on the B3LYP-D3BJ optimized geometries using ORCA 6.0.0. States with fosc (oscillation strength) > 0.01 are shown only. The orbitals with contribution > 0.05 are shown only in the state.

State	Wavelength (nm)	fosc (au**2)	Orbitals (contribution>0.05)	Transition
1	548	0.265	**640a (HOMO) -> 641a (LUMO)** (0.98)	MMLCT
3	483	0.054	**640a (HOMO)** -> 643a (0.98)	MMLCT
8	394	0.016	638a -> **641a (LUMO)** (0.13) 639a -> 642a (0.70) **640a (HOMO)** -> 645a (0.11)	LLCT+ dσ(Ir–Ir) -> dσ*(Ir–Ir)
10	389	1.040	639a -> 642a (0.11) **640a (HOMO)** -> 645a (0.74)	LLCT
exp	340/397/531			

† The corresponding orbitals can be visualized in Figure S54.

Table S23 The key emission calculations including SOC from triplet **A-I** (TDA:TRUE) and composition of each state in acetonitrile solvent by the CPCM TD-B3LYP-D3//B3LYP-D3BJ method based on the B3LYP-D3BJ optimized geometries using ORCA 6.0.0 The root with weight > 0.005 are shown only in the state.

State	Wavelength (nm)	Weight (>0.05)	Root	Spin	Ms	fosc (au**2)	Orbitals
14	646	0.57572	6	1	0	0.00018	434a -> 436a
		0.19246	6	1	-1		
		0.19246	6	1	1		
15	646	0.36283	6	1	0	0.00117	434a -> 436a
		0.31411	6	1	-1		
		0.31411	6	1	1		
16	646	0.46069	6	1	-1	0.00382	434a -> 436a
		0.46069	6	1	1		
17	642	0.07367	2	1	-1	0.00000	427a -> 435a
		0.21638	5	1	-1		433a -> 435a
		0.15984	7	1	-1		430a -> 435a
		0.07367	2	1	1		434a -> 437a
		0.21638	5	1	1		
		0.15984	7	1	1		
18	637	0.75665	7	0	1	0.00000	434a -> 437a
		0.10740	7	-1	1		
		0.10740	7	1	1		
19	634	0.13380	7	1	0	0.00000	430a -> 435a
		0.05084	5	1	-1		434a -> 437a
		0.34950	7	1	-1		
		0.05084	5	1	1		
		0.34950	7	1	1		
Exp	629/642						

† The corresponding orbitals can be visualized in Figure S56.

Table S24 The key emission calculations including SOC from triplet **A-SCN** (TDA:TRUE) and composition of each state in acetonitrile solvent by the CPCM TD-B3LYP-D3//B3LYP-D3BJ method based on the B3LYP-D3BJ optimized geometries using ORCA 6.0.0 The root with weight > 0.005 are shown only in the state.

State	Wavelength (nm)	Weight	Root	Spin	Ms	fosc (au**2)	Orbitals
5	670	0.46758	2	1	-1	0.00081	405a -> 411a
		0.46758	2	1	1		409a -> 411a
6	667	0.84106	2	1	0	0.00002	405a -> 411a
		0.06414	2	1	-1		409a -> 411a
		0.06414	2	1	1		
7	657	0.48987	3	1	-1	0.00000	404a -> 411a
		0.48987	3	1	1		408a -> 411a
8	655	0.91441	3	1	0	0.00000	404a -> 411a
							408a -> 411a
9	642	0.06919	3	1	0	0.00000	404a -> 411a
		0.43629	3	1	-1		408a -> 411a
		0.43629	3	1	1		
13	554	0.22503	4	1	0	0.00013	410a -> 413a
		0.38462	4	1	-1		
		0.38462	4	1	1		
14	553	0.74630	4	1	0	0.00000	410a -> 413a
		0.12633	4	1	-1		
		0.12633	4	1	1		
15	553	0.46356	4	1	-1	0.00634	410a -> 413a
		0.46356	4	1	1		
Exp	581/676						

† The corresponding orbitals can be visualized in Figure S57.

Table S25 The key emission calculations including SOC from triplet **A-POMe** (TDA:TRUE) and composition of each state in acetonitrile solvent by the CPCM TD-B3LYP-D3//B3LYP-D3BJ method based on the B3LYP-D3BJ optimized geometries using ORCA 6.0.0 The root with weight > 0.005 are shown only in the state.

State	Wavelength (nm)	Weight	Root	Spin	Ms	fosc (au**2)	Orbitals
5	668	0.73220	2	1	0	0.00000	640a -> 642a
		0.13259	2	1	-1		
		0.13259	2	1	1		
6	668	0.20397	2	1	0	0.00000	640a -> 642a
		0.39671	2	1	-1		
		0.39671	2	1	1		
7	668	0.06129	2	1	0	0.00000	640a -> 642a
		0.46876	2	1	-1		
		0.46876	2	1	1		
8	628	0.46919	3	1	-1	0.00000	640a -> 643a 640a -> 645a
		0.46919	3	1	1		
9	628	0.19138	3	1	0	0.00064	640a -> 643a 640a -> 645a
		0.39091	3	1	-1		
		0.39091	3	1	-1		
10	628	0.76018	3	1	0	0.00109	640a -> 643a 640a -> 645a
		0.11628	3	1	-1		
		0.11628	3	1	1		
Exp	648/644/620						

† The corresponding orbitals can be visualized in Figure S58.

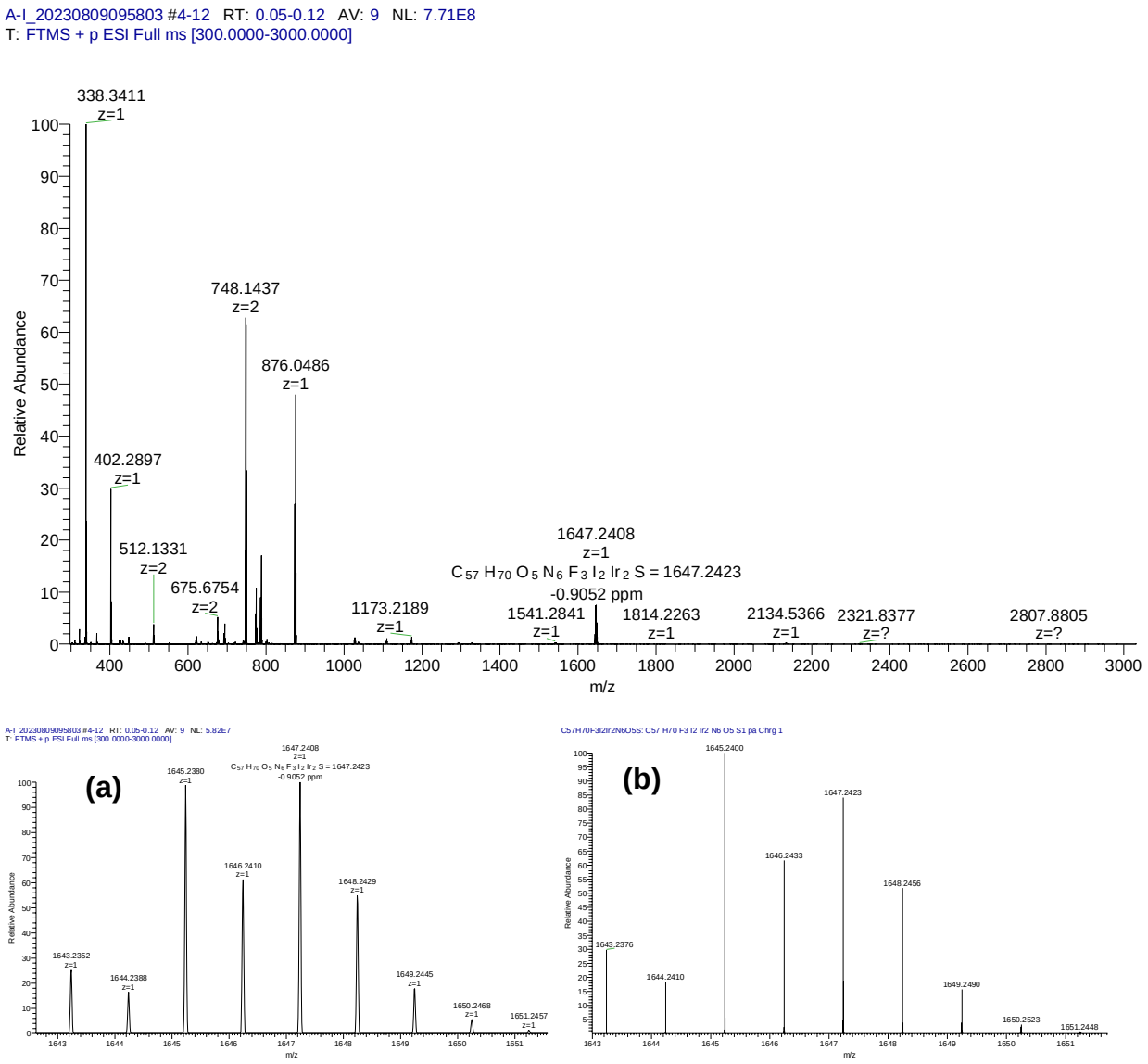

Figure S1. (Top) HRMS (ESI) spectrum of complex **A-I** (Bottom) Expanded peak at m/z = 1647 (a) and theoretical isotope pattern of $[M - OTf^-]^+$ (b).

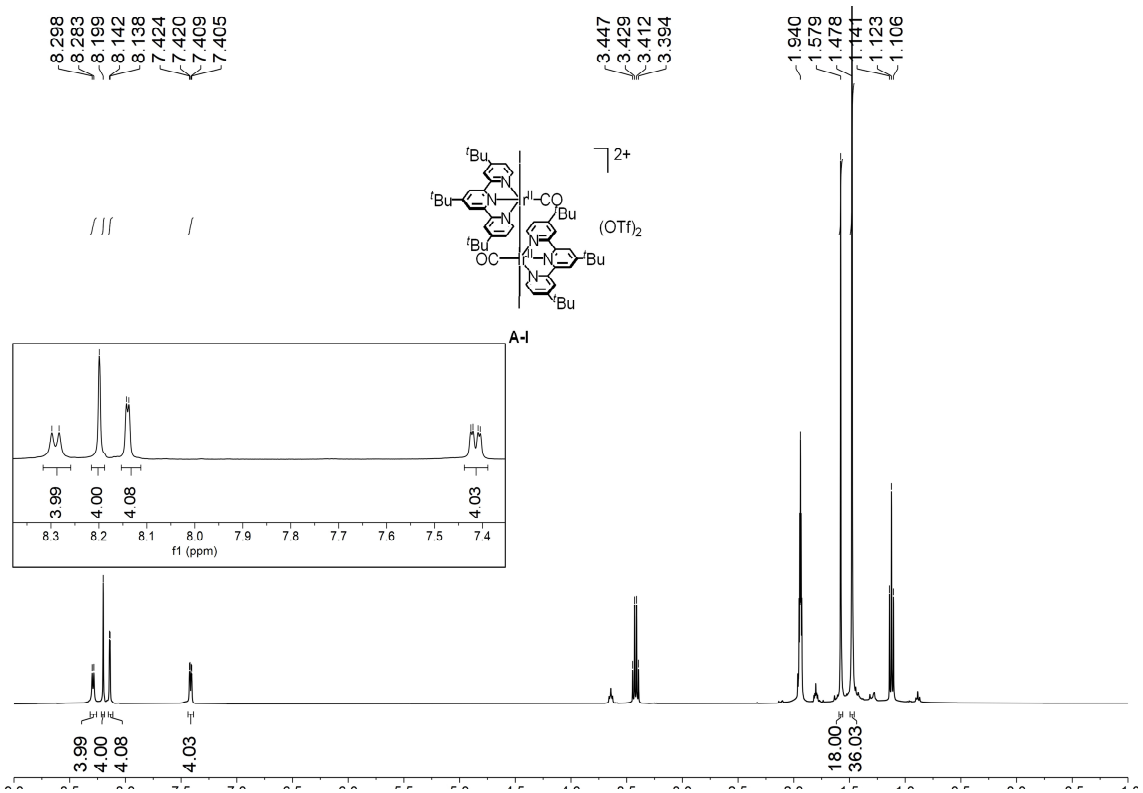

Figure S2. ^{1}H NMR spectrum of complex **A-I** in CD_3CN.

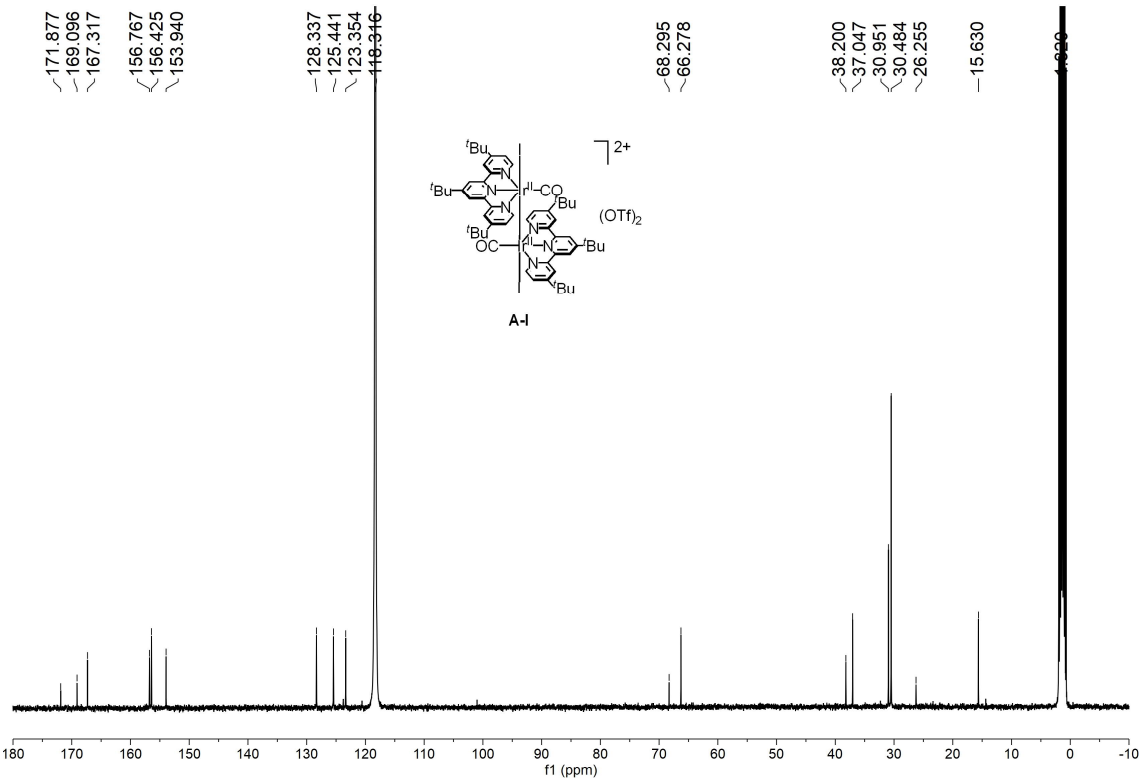

Figure S3. ^{13}C NMR spectrum of complex **A-I** in CD_3CN.

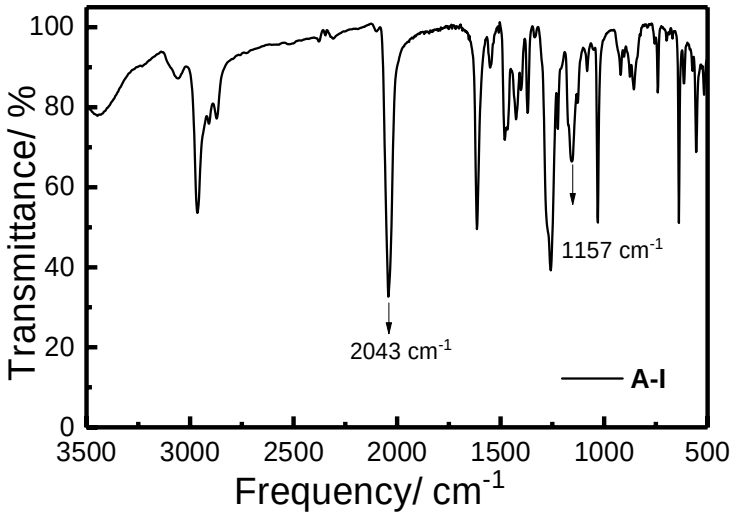

Figure S4. IR spectrum of complex **A-I** in KBr showing ν(C≡O) and ν(S=O) stretching.

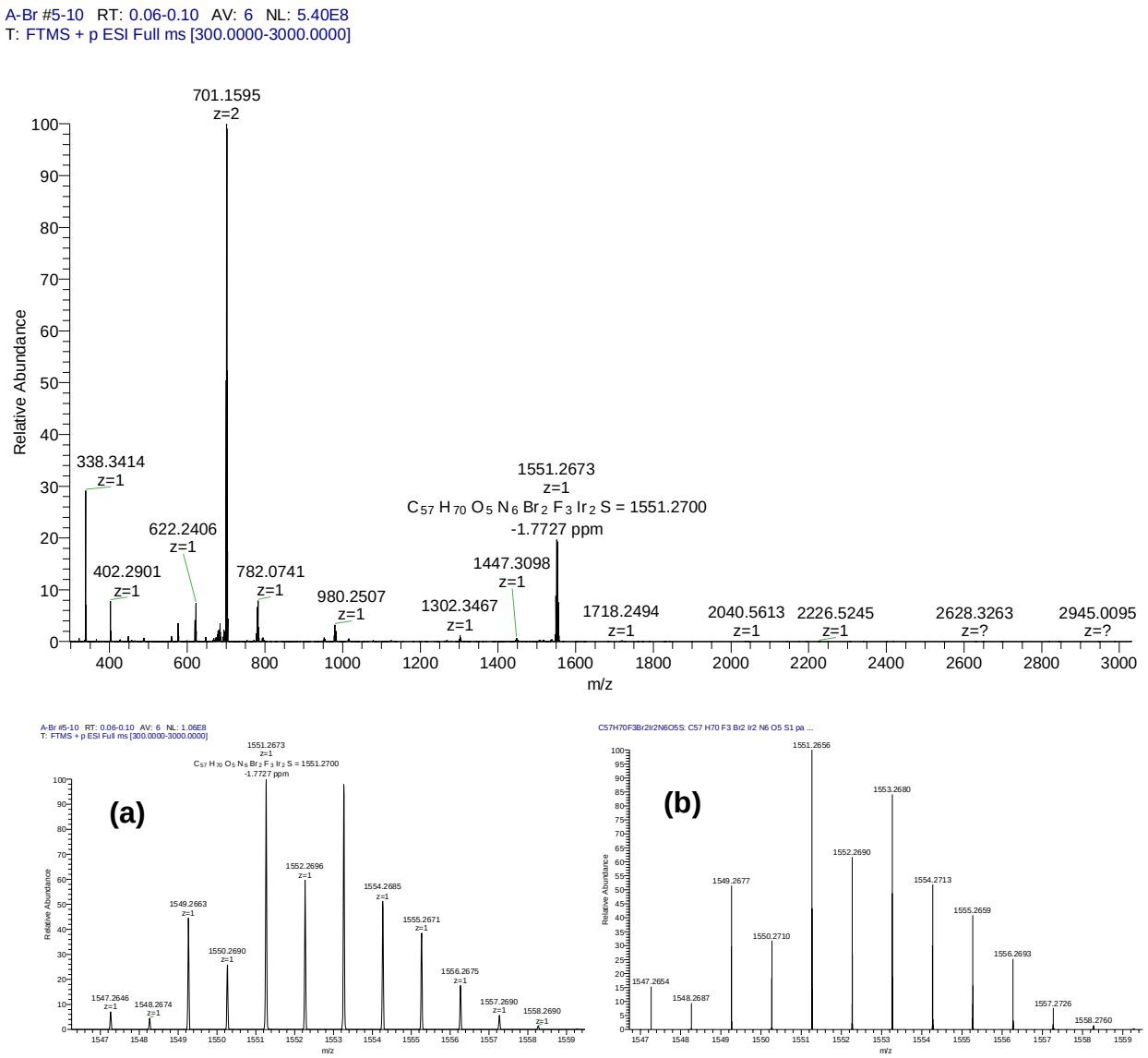

Figure S5. (Top) HRMS (ESI) spectrum of complex **A-Br** (Bottom) Expanded peak at m/z = 1551 (a) and theoretical isotope pattern of $[M – OTf^{–}]^{+}$ (b).

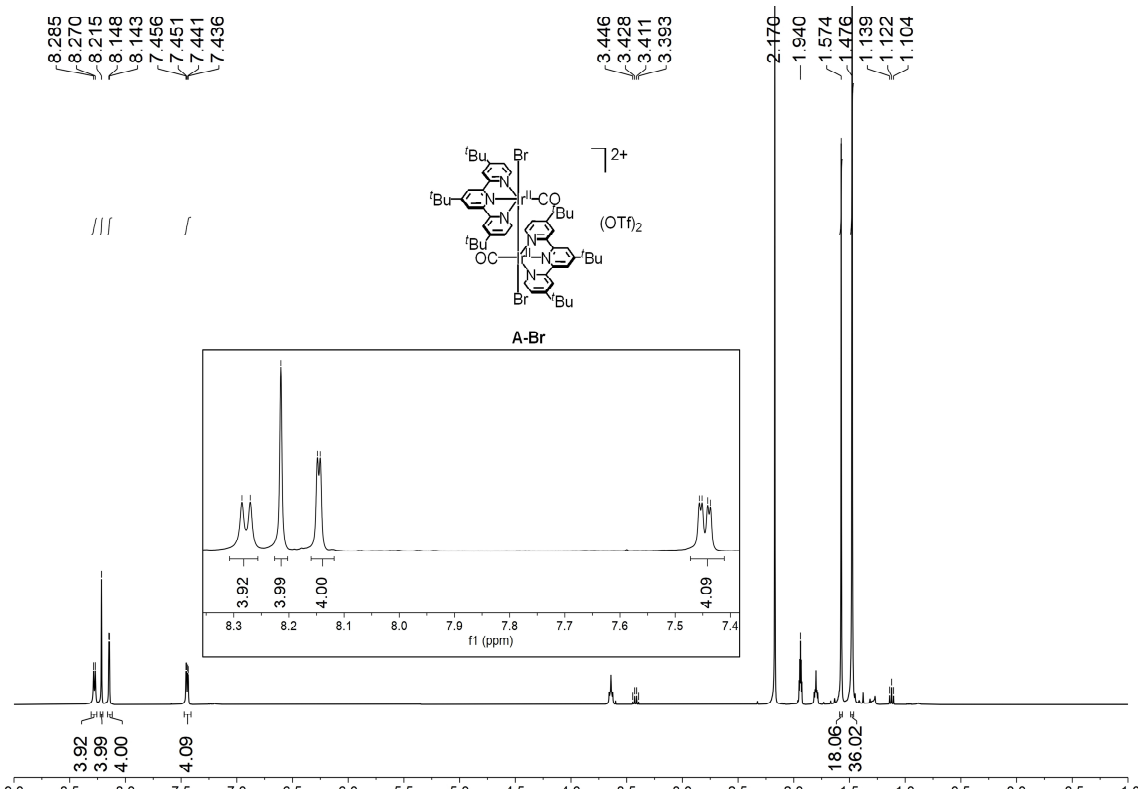

Figure S6. ^{1}H NMR spectrum of complex **A-Br** in CD_3CN.

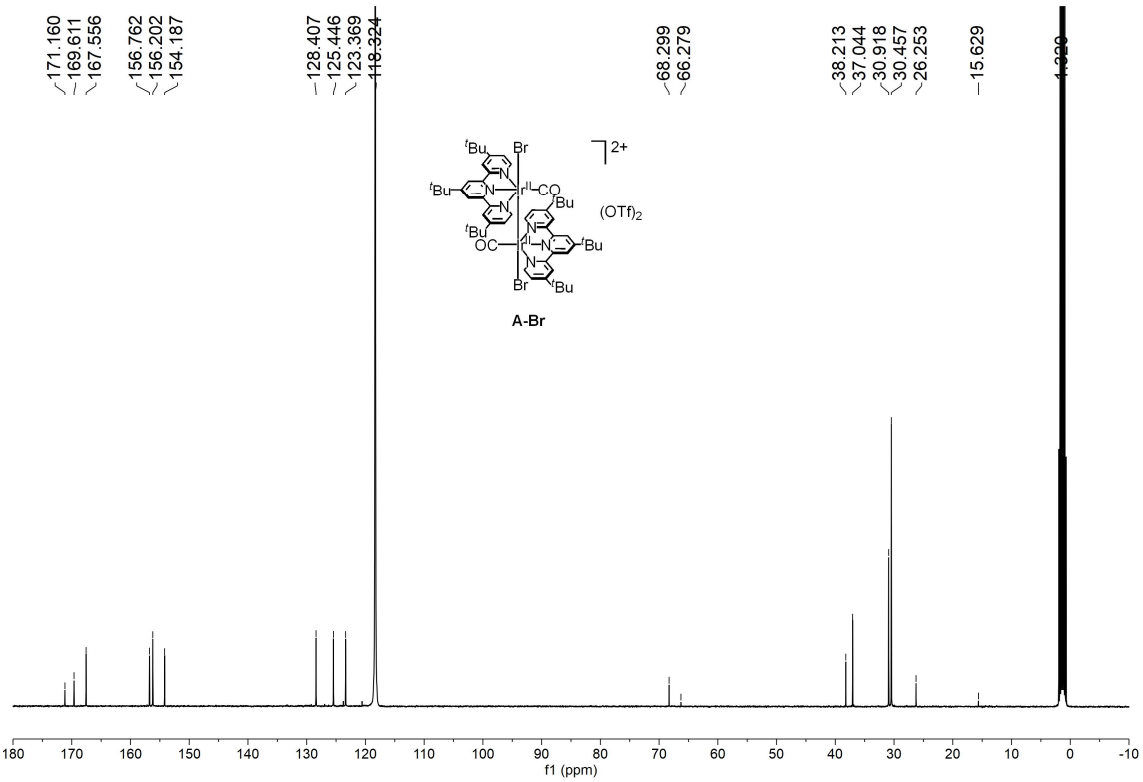

Figure S7. ^{13}C NMR spectrum of complex **A-Br** in CD_3CN.

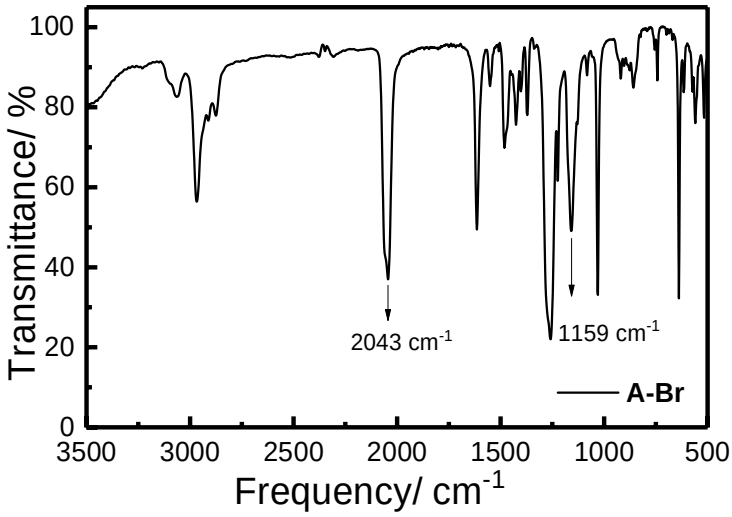

Figure S8. IR spectrum of complex **A-Br** in KBr showing ν(C≡O) and ν(S=O) stretching.

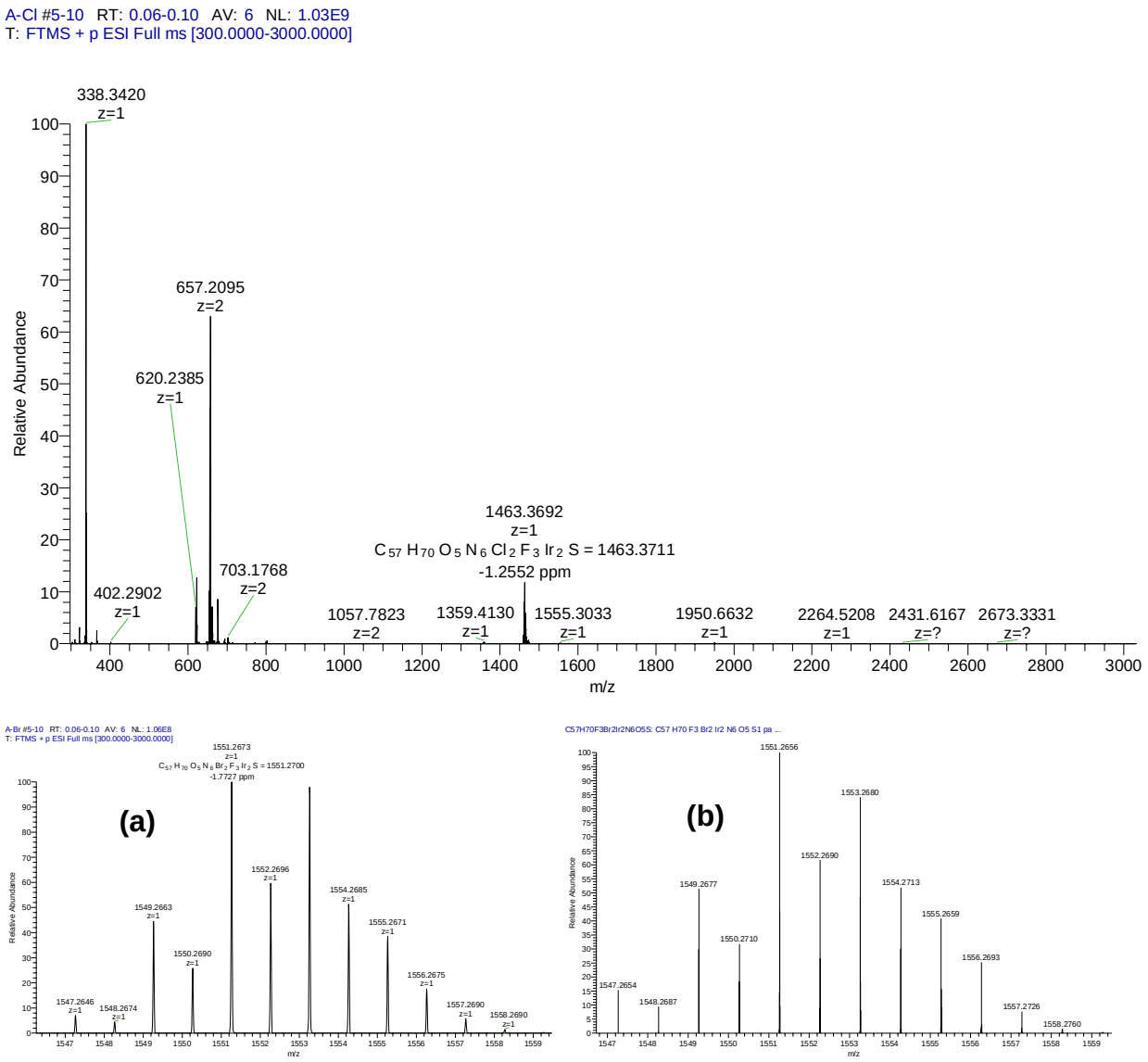

Figure S9. (Top) HRMS (ESI) spectrum of complex **A-Cl** (Bottom) Expanded peak at m/z = 1463 (a) and theoretical isotope pattern of $[M - OTf^-]^+$ (b).

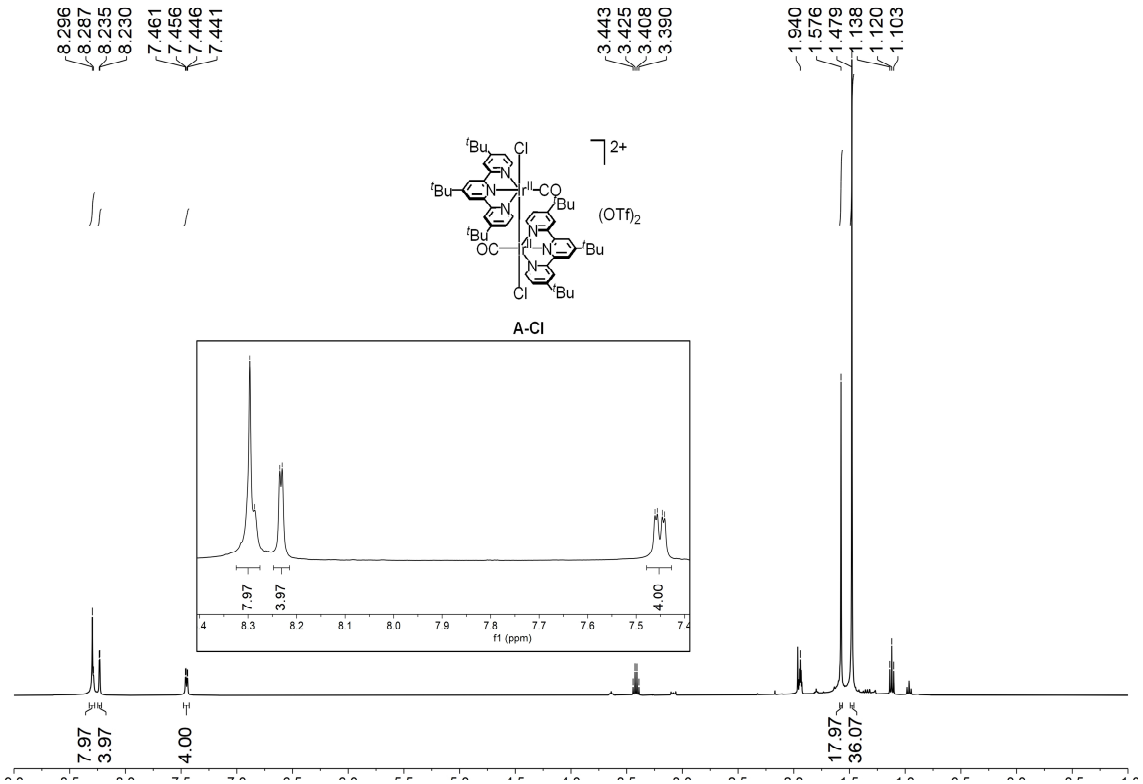

Figure S10. ^{1}H NMR spectrum of complex **A-Cl** in CD_3CN.

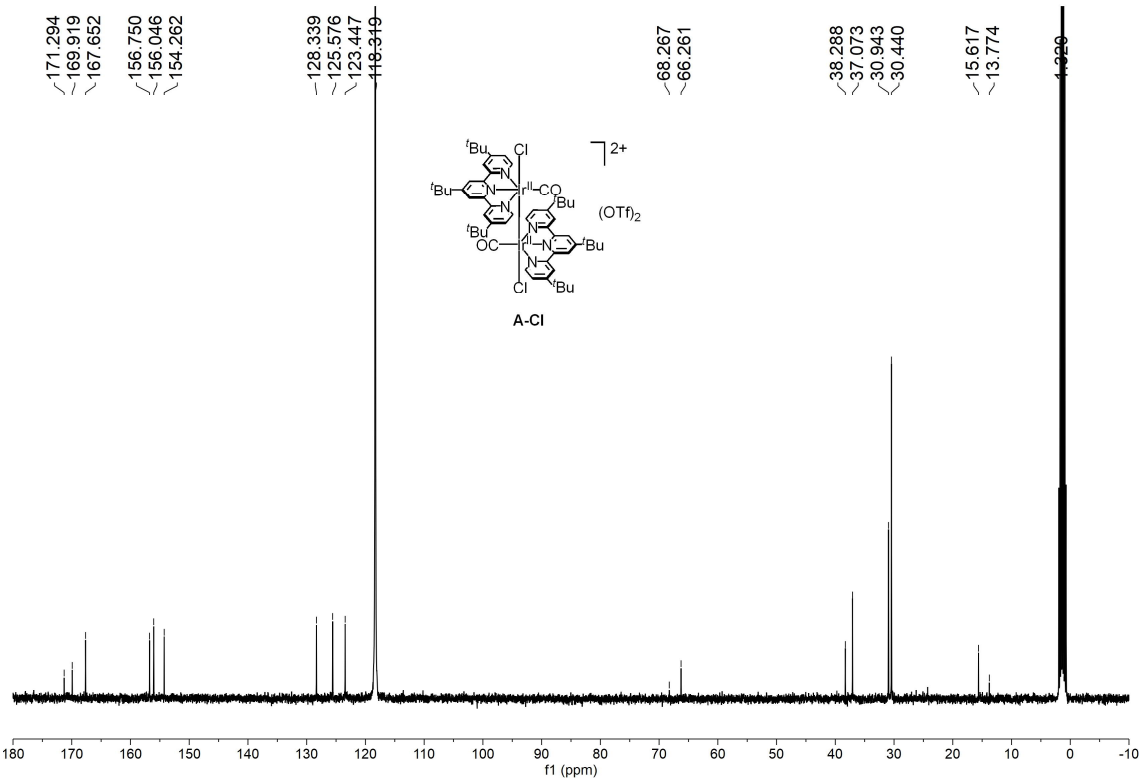

Figure S11. ^{13}C NMR spectrum of complex **A-Cl** in CD_3CN.

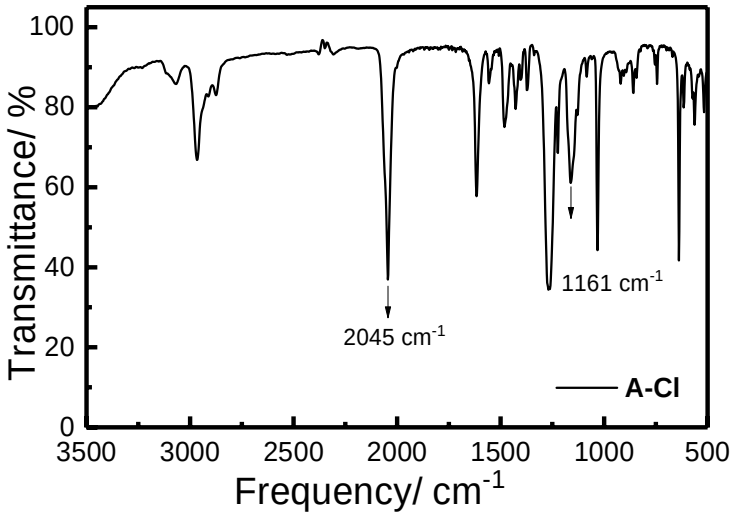

Figure S12. IR spectrum of complex **A-Cl** in KBr showing ν(C≡O) and ν(S=O) stretching.

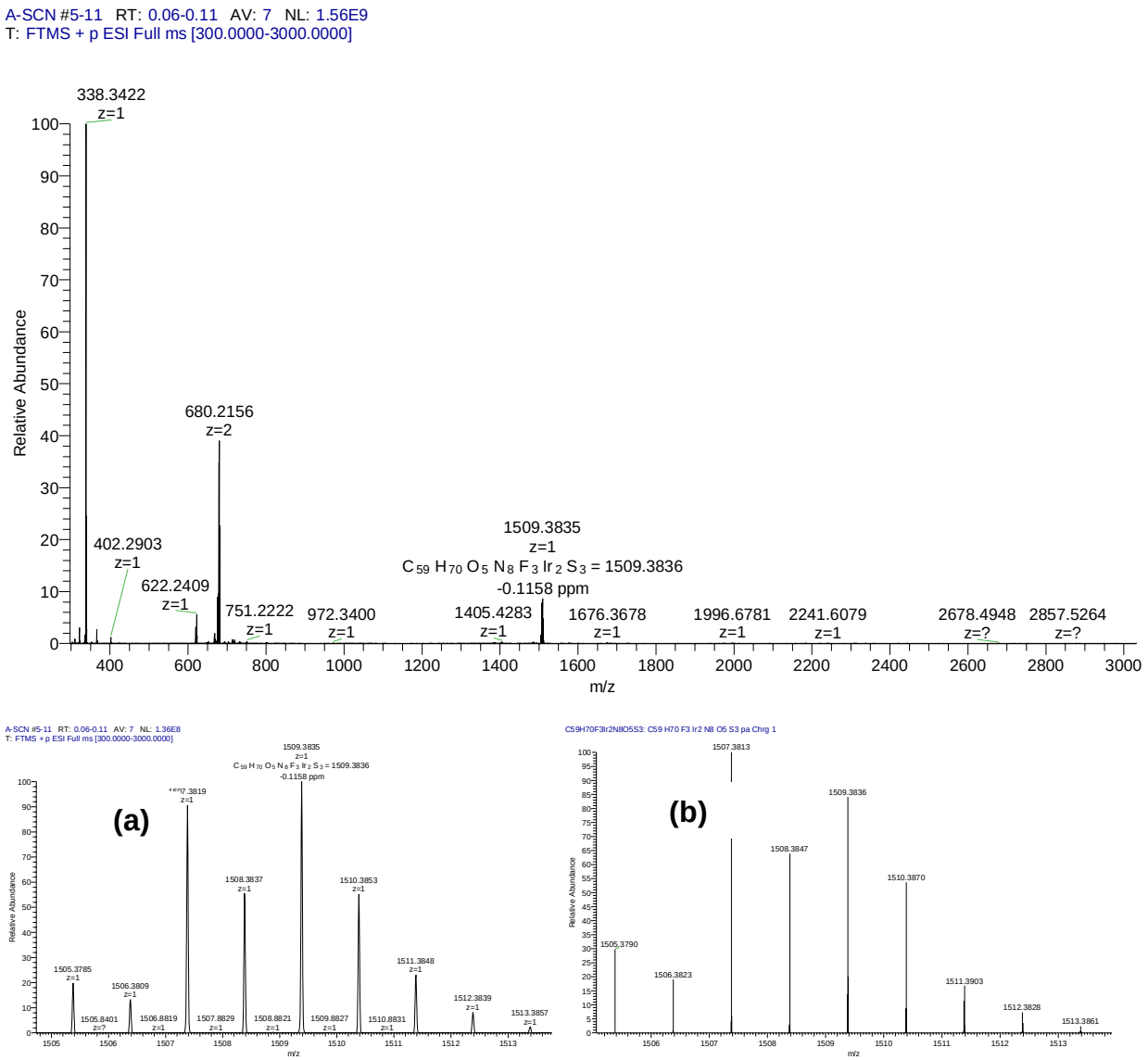

Figure S13. (Top) HRMS (ESI) spectrum of complex **A-SCN** (Bottom) Expanded peak at m/z = 1509 (a) and theoretical isotope pattern of $[M – OTf^{–}]^{+}$ (b).

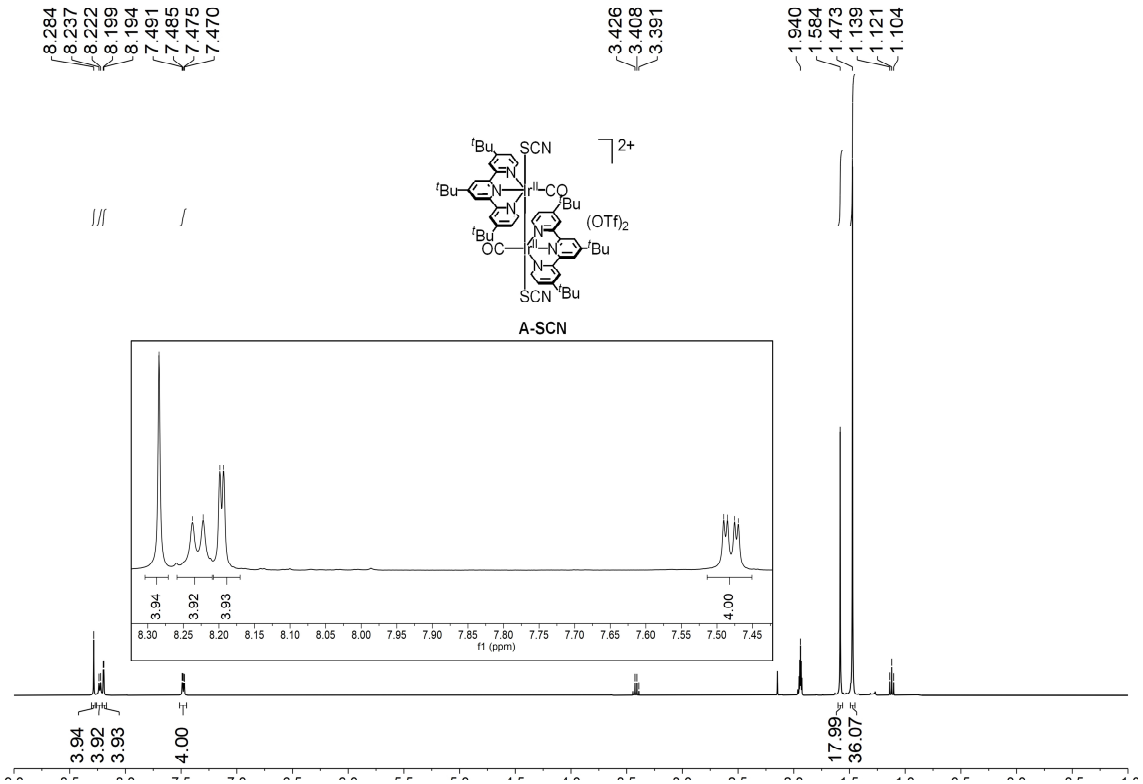

Figure S14. ^{1}H NMR spectrum of complex **A-SCN** in CD_3CN.

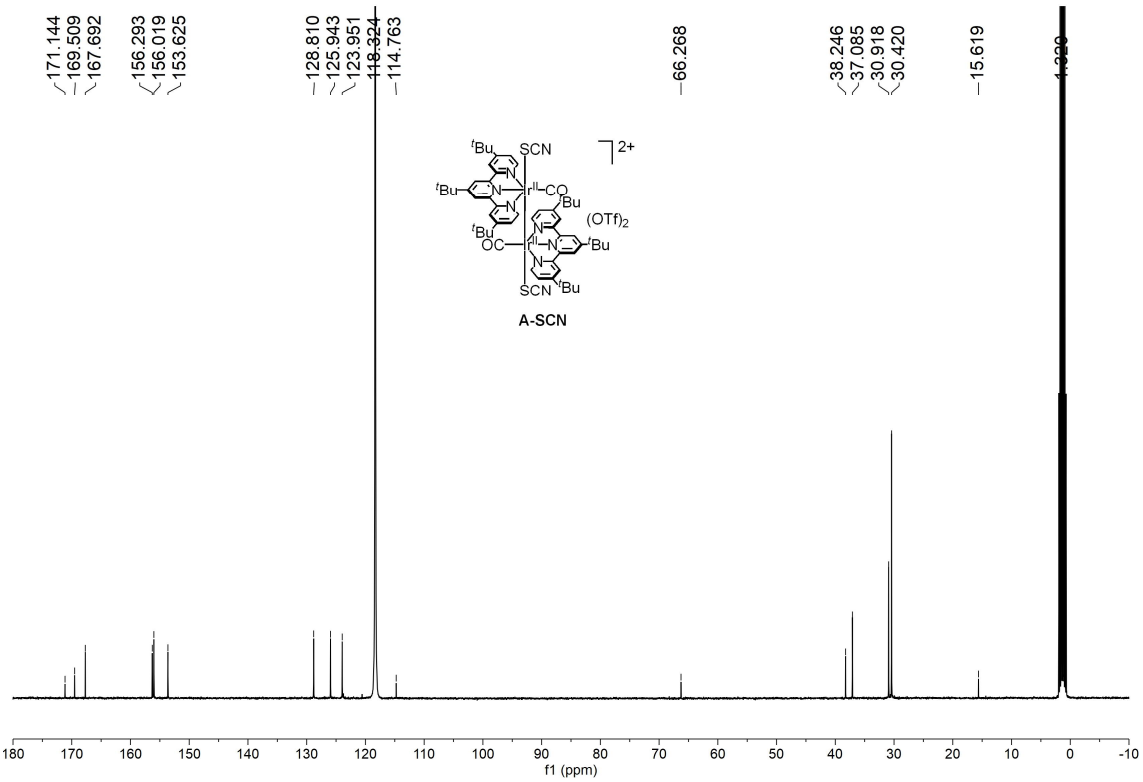

Figure S15. ^{13}C NMR spectrum of complex **A-SCN** in CD_3CN.

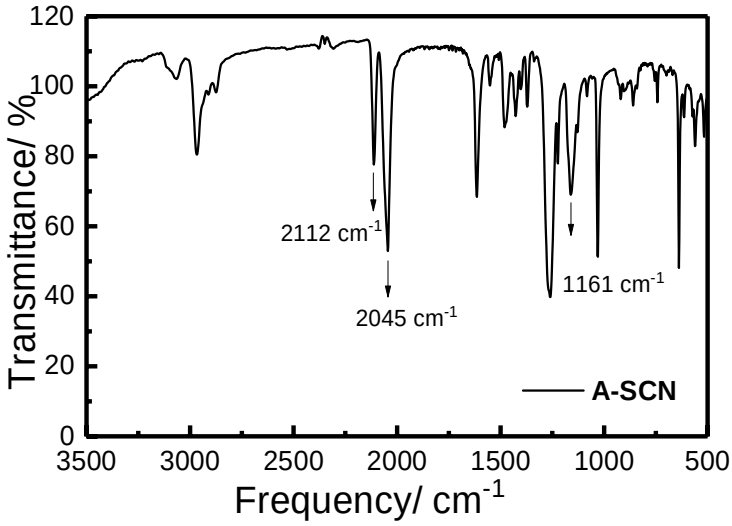

Figure S16. IR spectrum of complex **A-SCN** in KBr showing ν(C≡O), ν(S–C≡N) and ν(S=O) stretching.

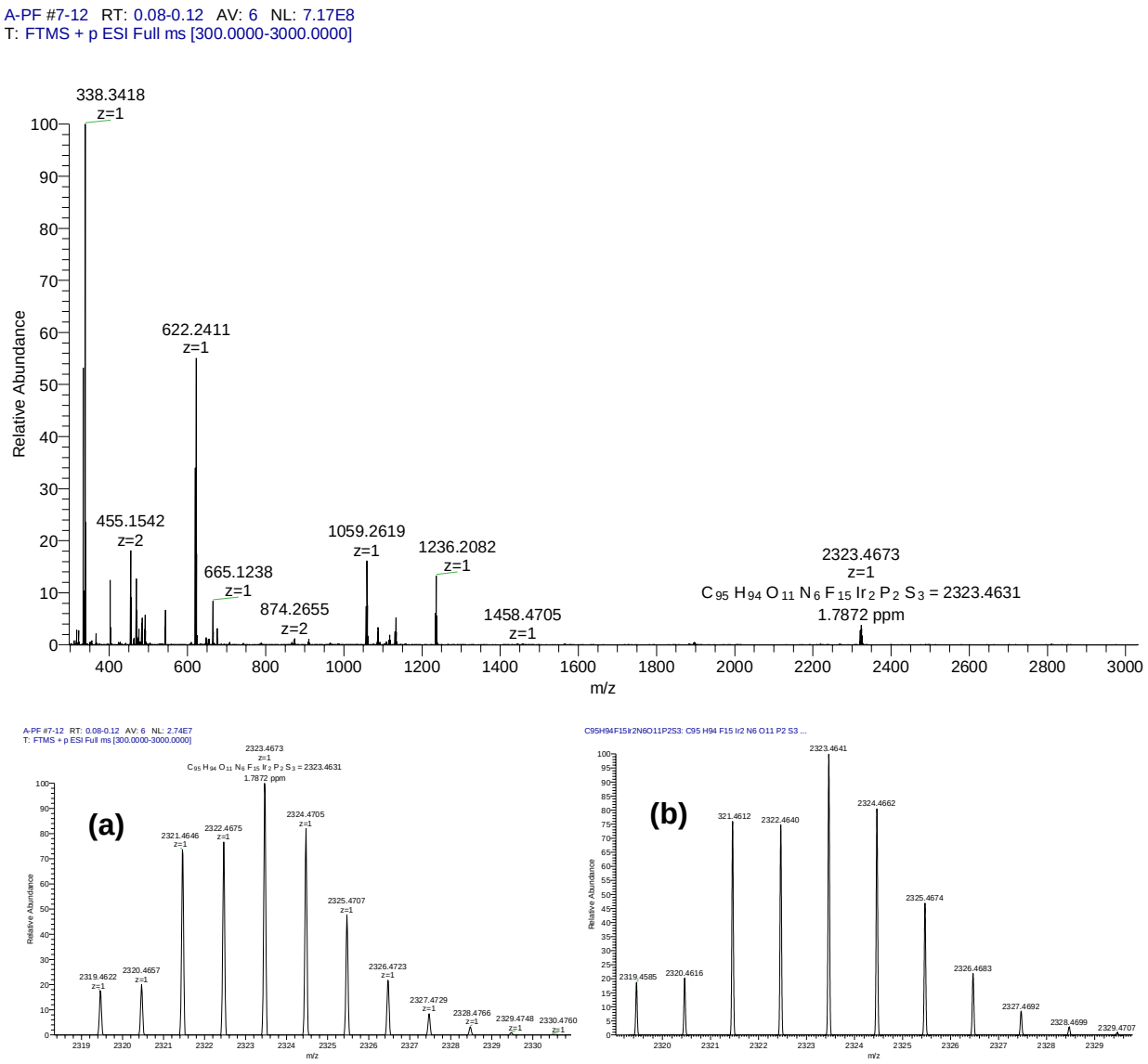

Figure S17. (Top) HRMS (ESI) spectrum of complex **A-PF** (Bottom) Expanded peak at m/z = 2323 (a) and theoretical isotope pattern of $[M - OTf^-]^+$ (b).

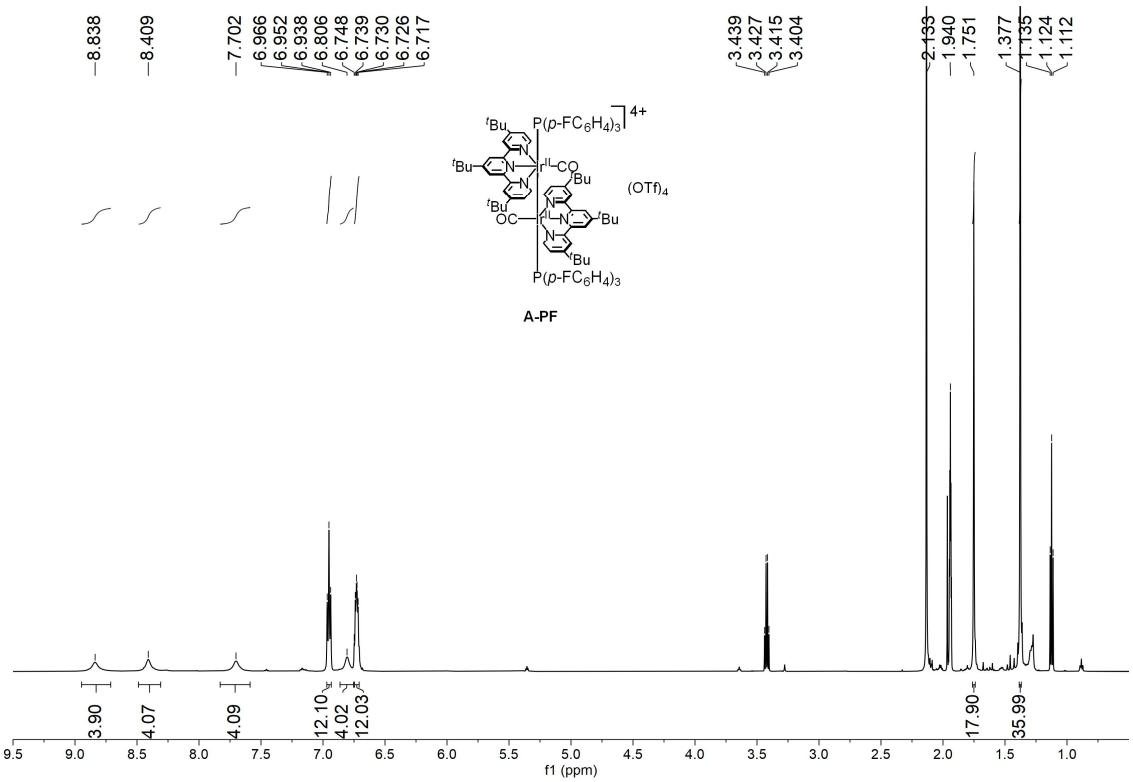

Figure S18. ^{1}H NMR spectrum of complex **A-PF** in CD_3CN.

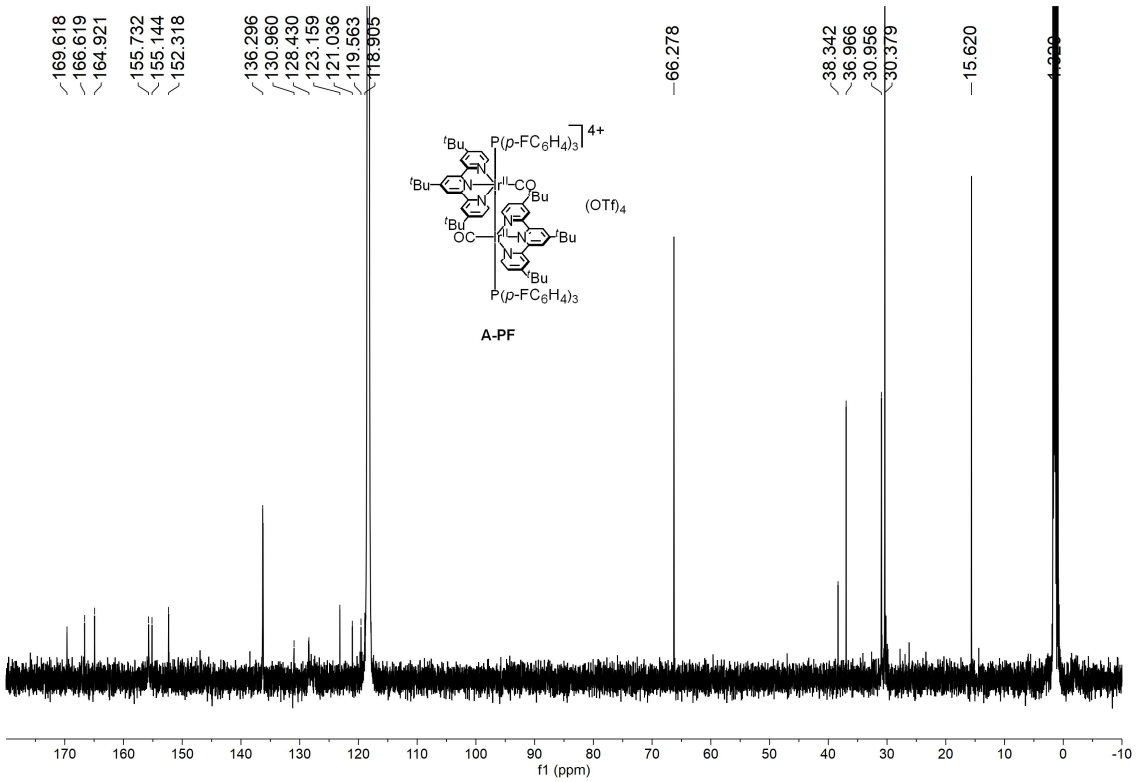

Figure S19. ^{13}C NMR spectrum of complex **A-PF** in CD_3CN.

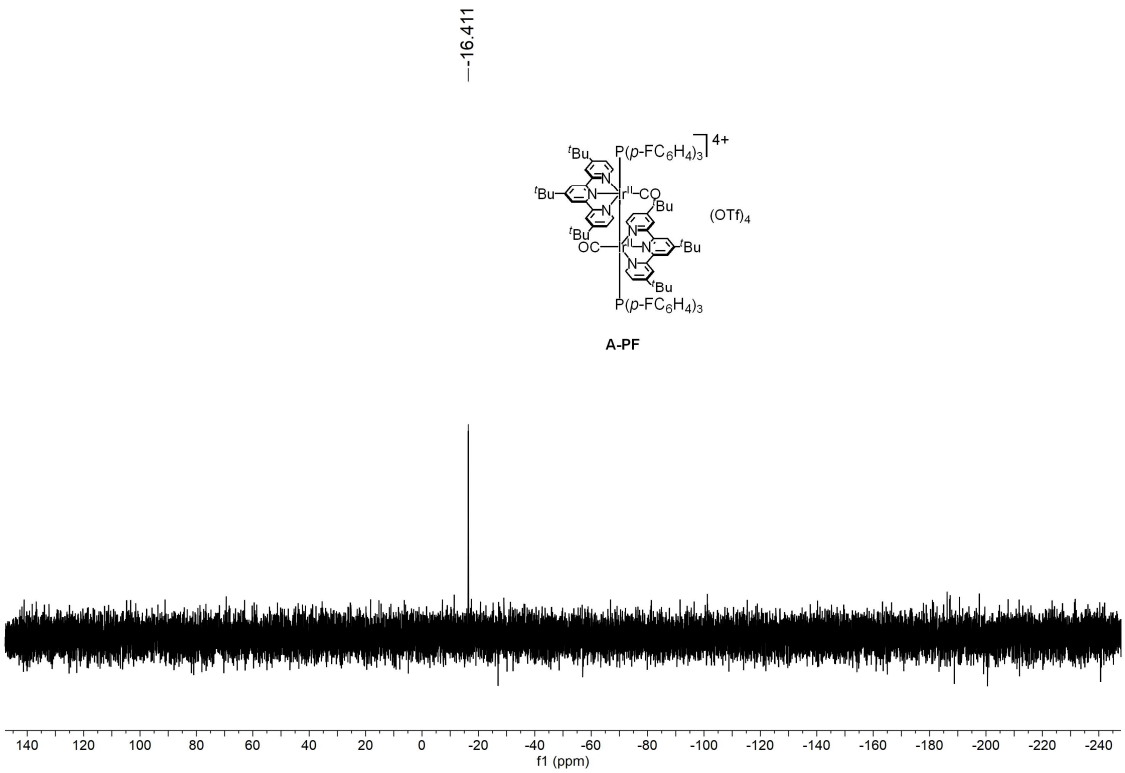

Figure S20. ^{31}P NMR spectrum of complex **A-PF** in CD3CN.

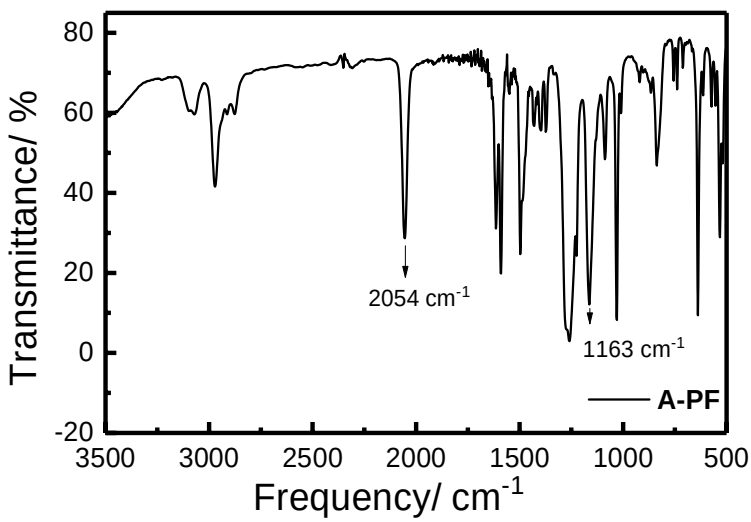

Figure S21. IR spectrum of complex **A-PF** in KBr showing ν(C≡O) and ν(S=O) stretching.

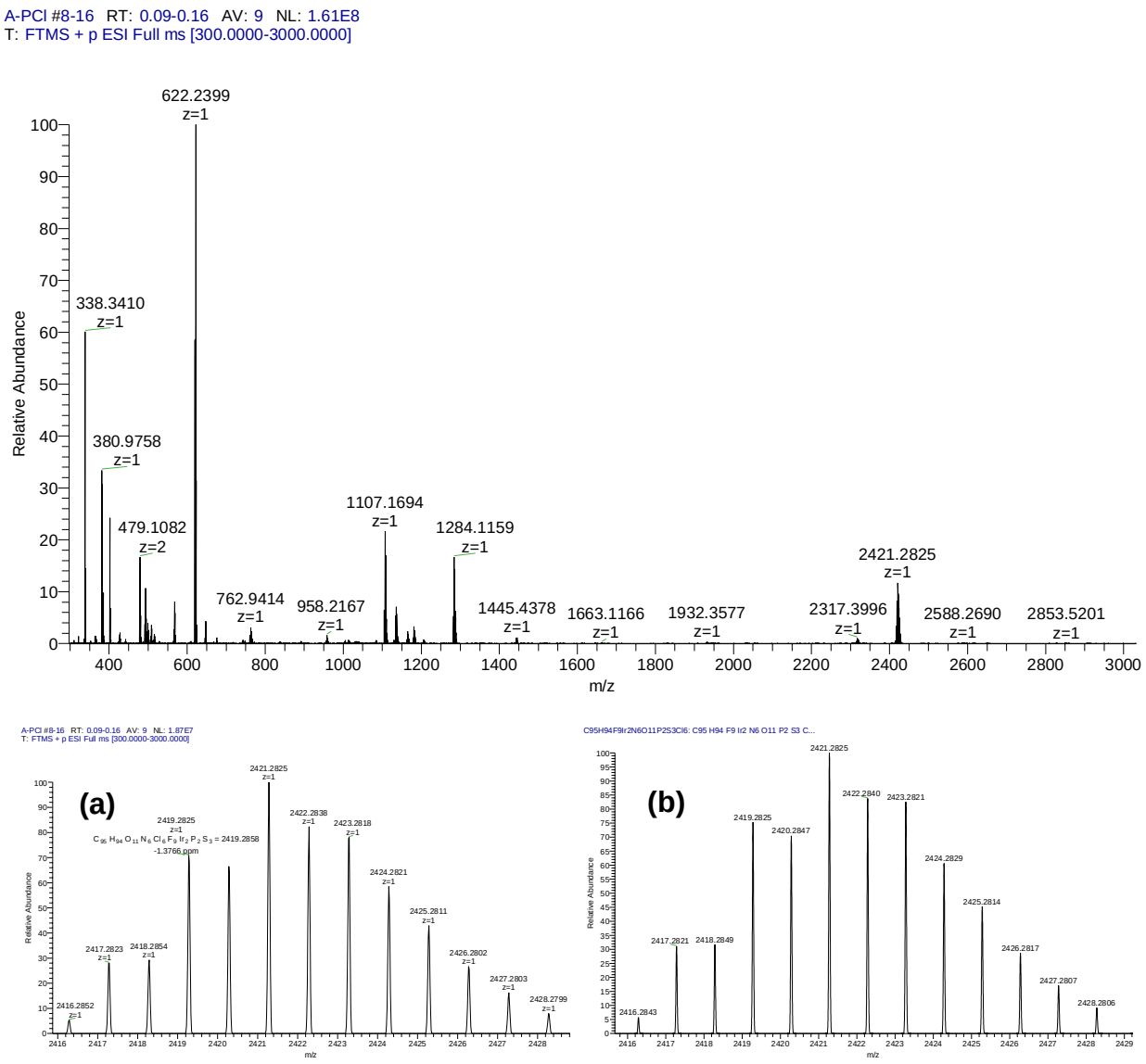

Figure S22. (Top) HRMS (ESI) spectrum of complex **A-PCl** (Bottom) Expanded peak at m/z = 2421 (a) and theoretical isotope pattern of $[M - OTf^-]^+$ (b).

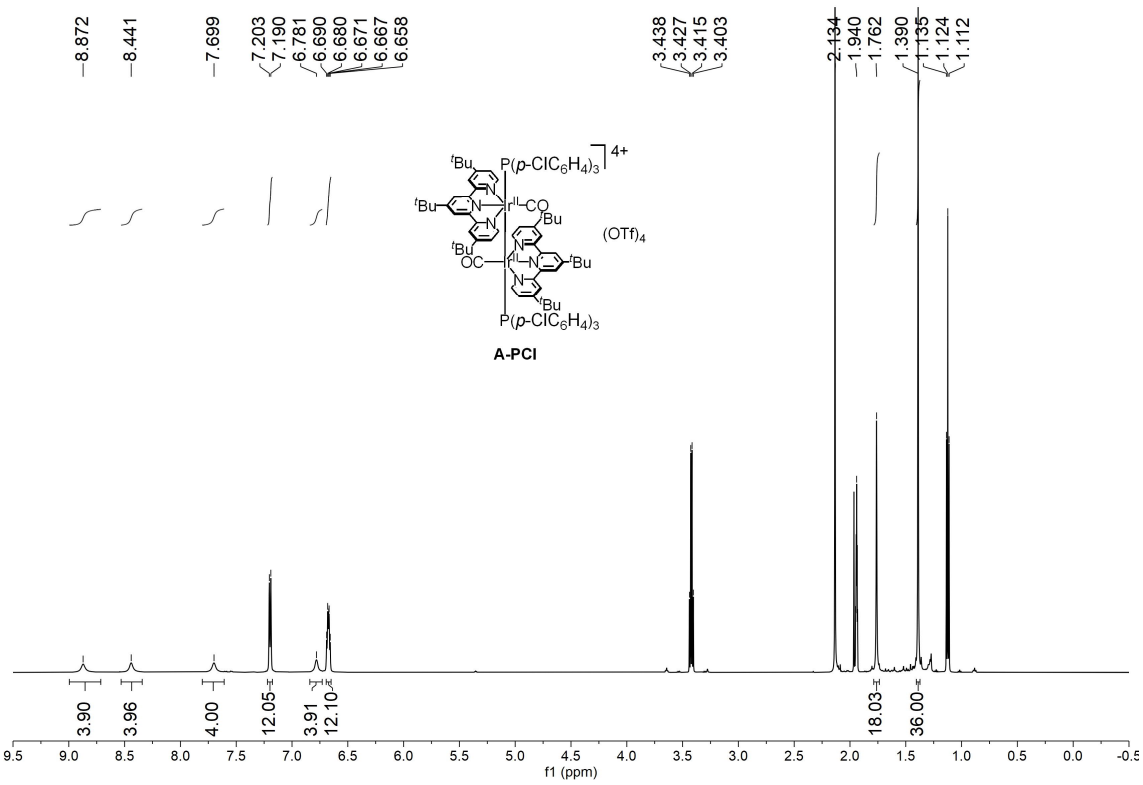

Figure S23. ^{1}H NMR spectrum of complex **A-PCl** in CD_3CN.

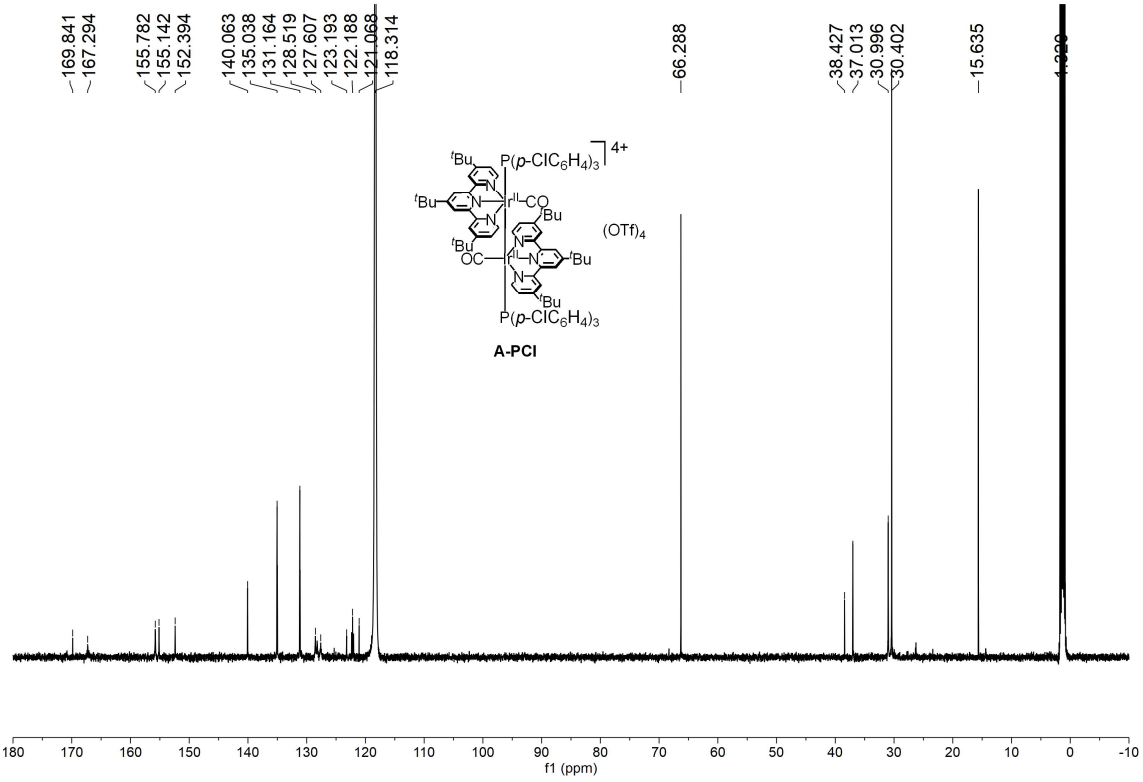

Figure S24. ^{13}C NMR spectrum of complex **A-PCl** in CD_3CN.

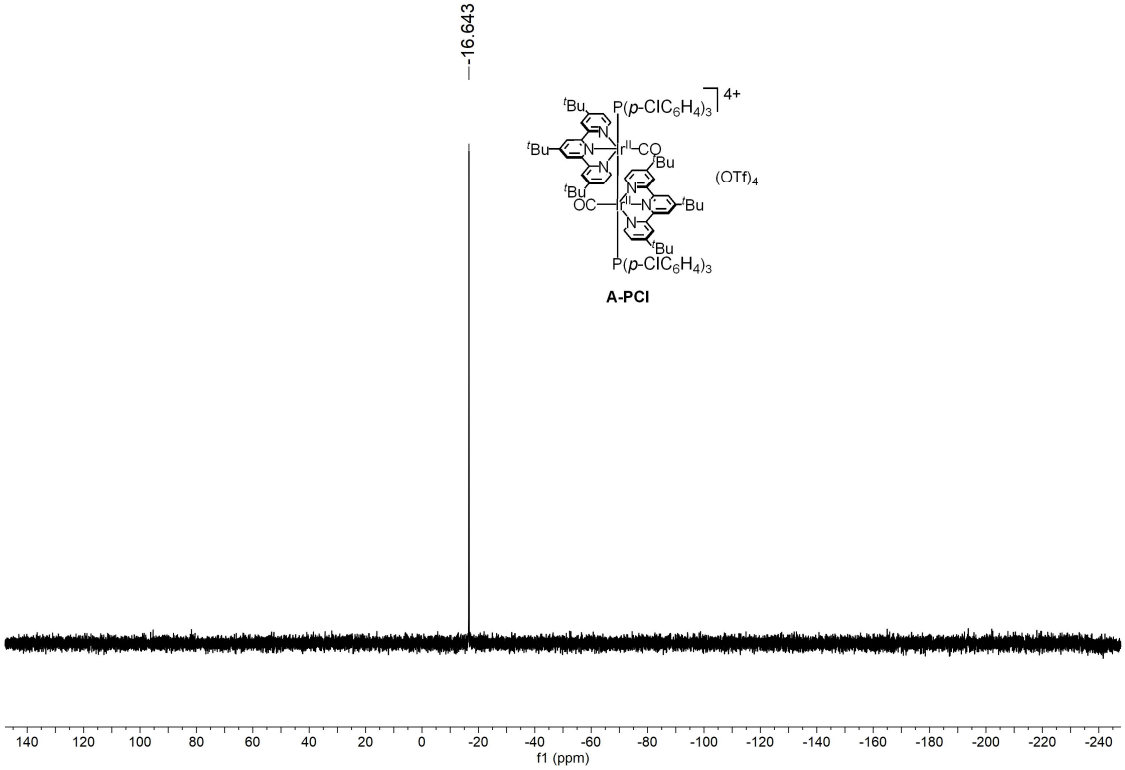

Figure S25. ^{31}P NMR spectrum of complex **A-PCl** in CD_3CN.

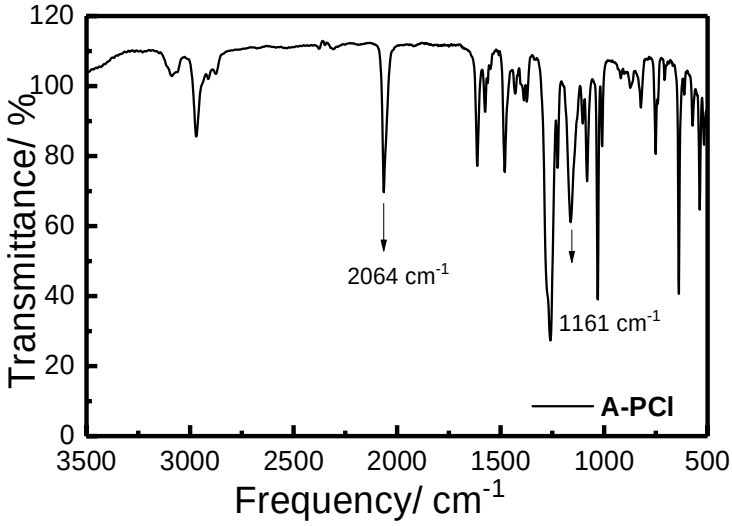

Figure S26. IR spectrum of complex **A-PCl** in KBr showing ν(C≡O) and ν(S=O) stretching.

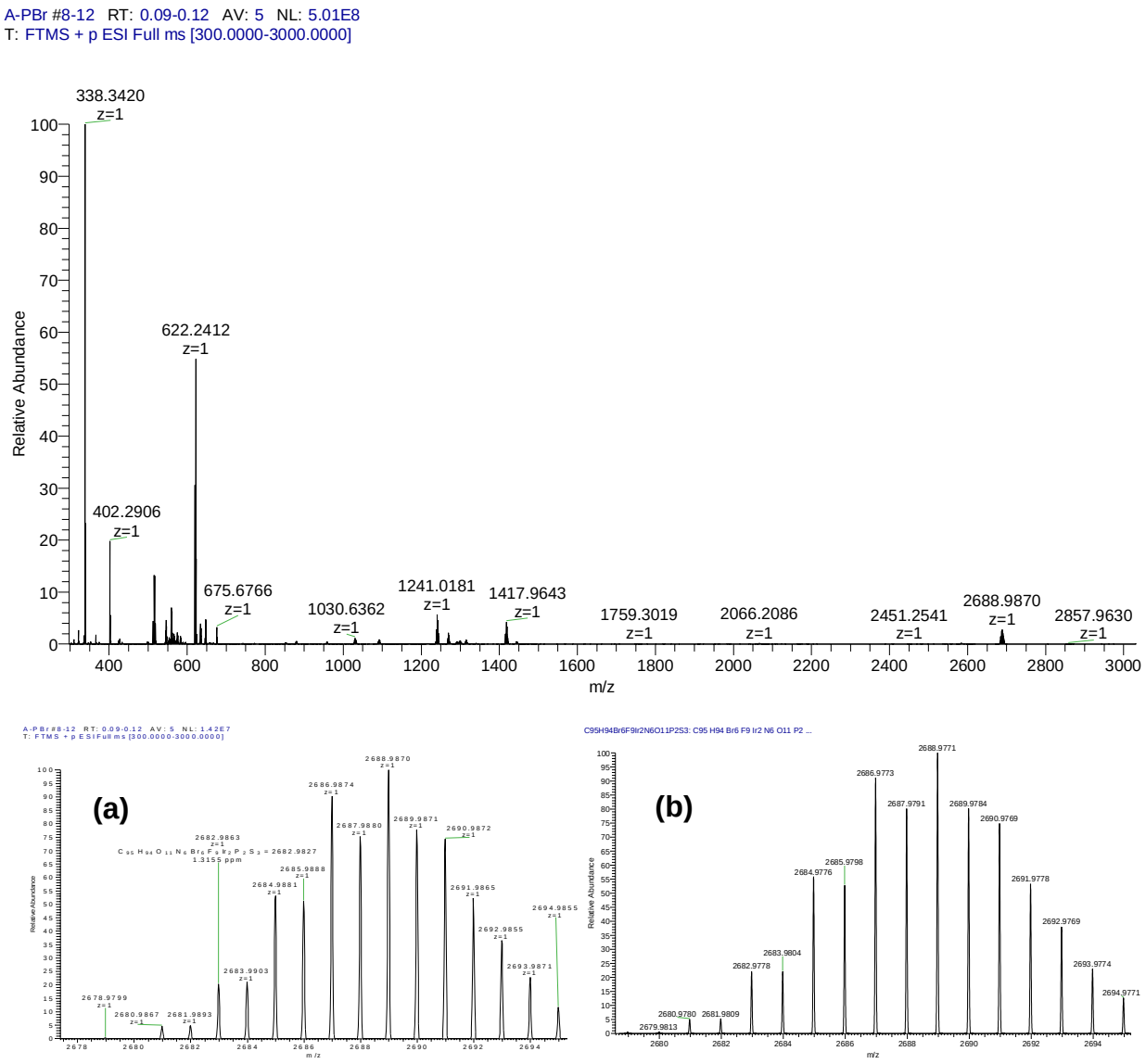

Figure S27. (Top) HRMS (ESI) spectrum of complex **A-PBr** (Bottom) Expanded peak at m/z = 2688 (a) and theoretical isotope pattern of $[M - OTf^-]^+$ (b).

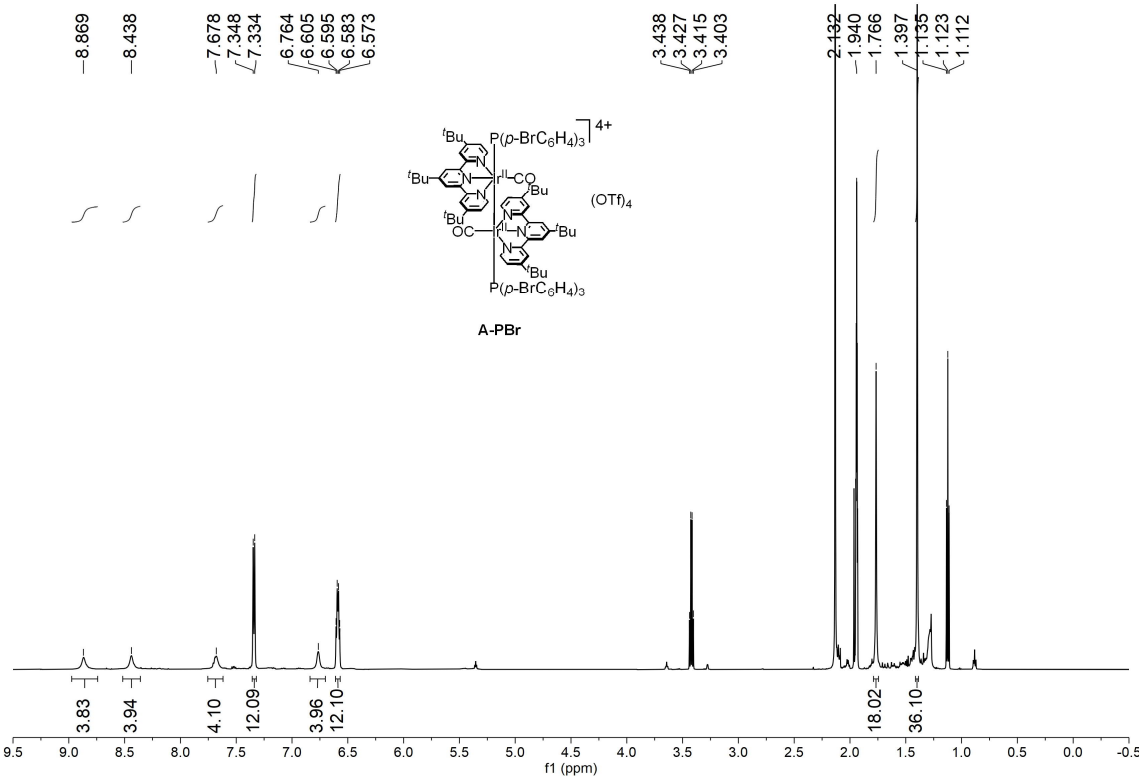

Figure S28. ^{1}H NMR spectrum of complex **A-PBr** in CD_3CN.

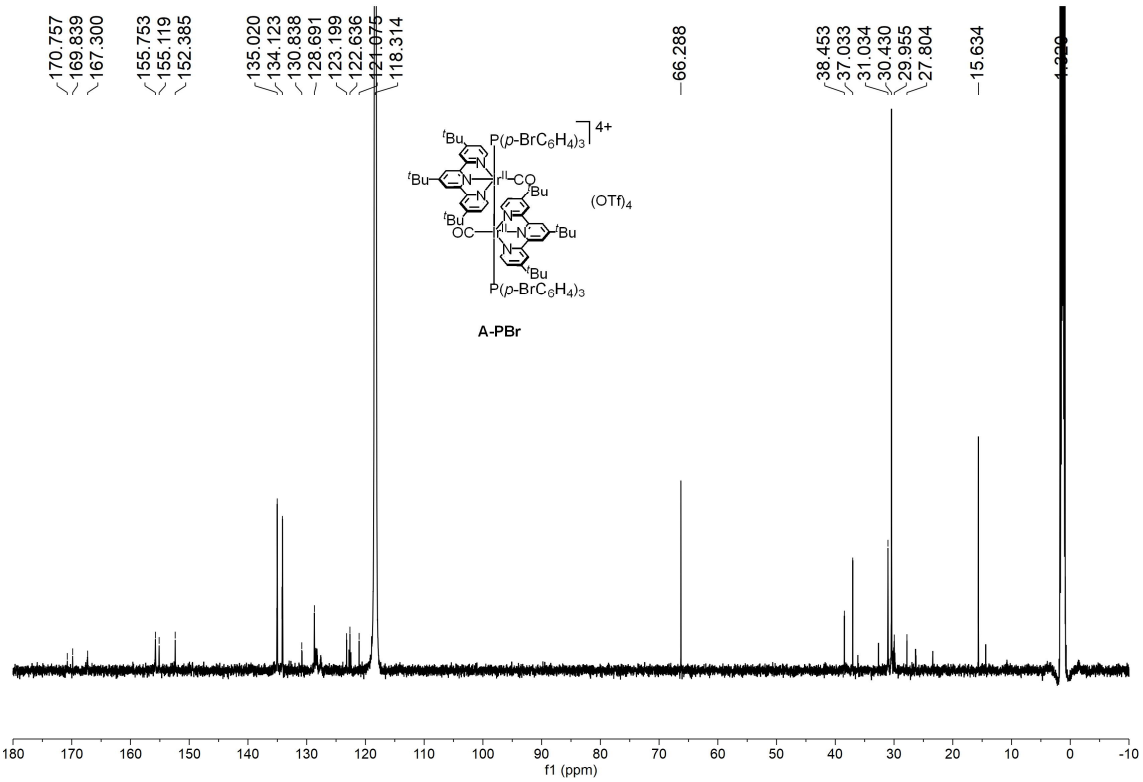

Figure S29. ^{13}C NMR spectrum of complex **A-PBr** in CD_3CN.

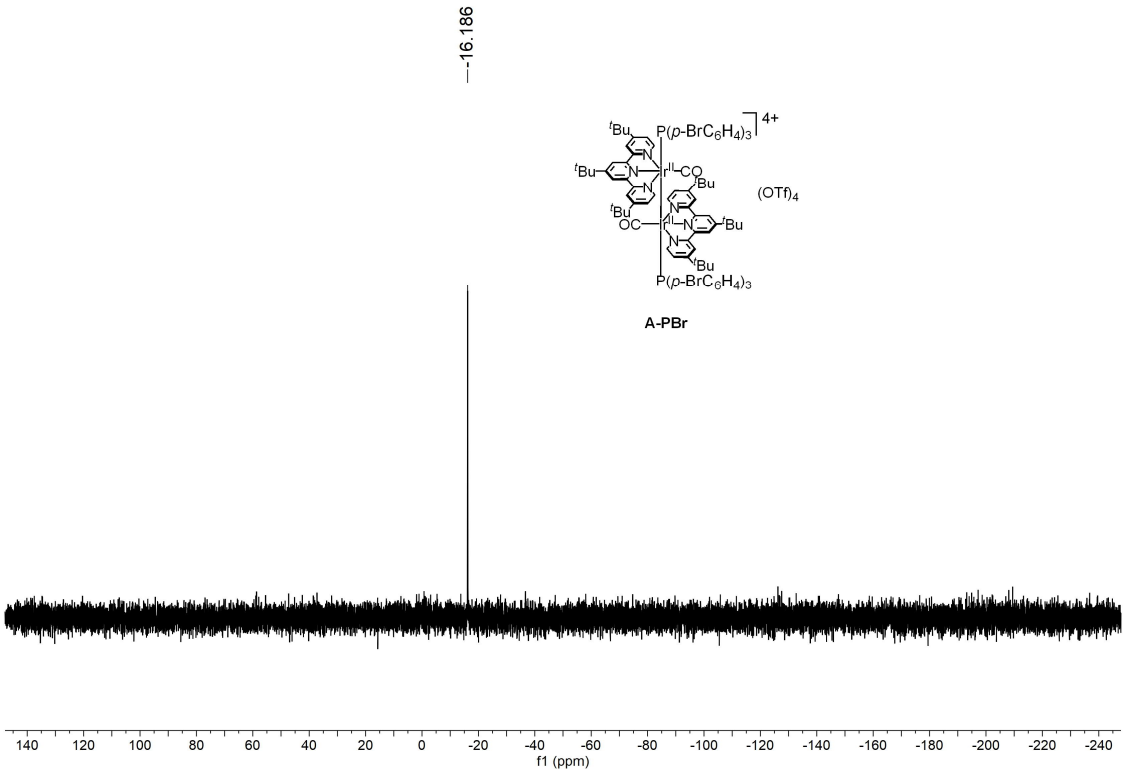

Figure S30. ^{31}P NMR spectrum of complex **A-PBr** in CD_3CN.

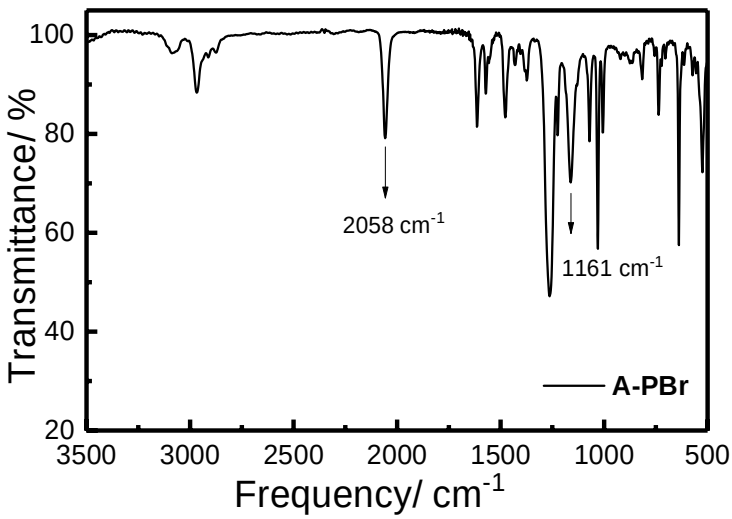

Figure S31. IR spectrum of complex **A-PBr** in KBr showing ν(C≡O) and ν(S=O) stretching.

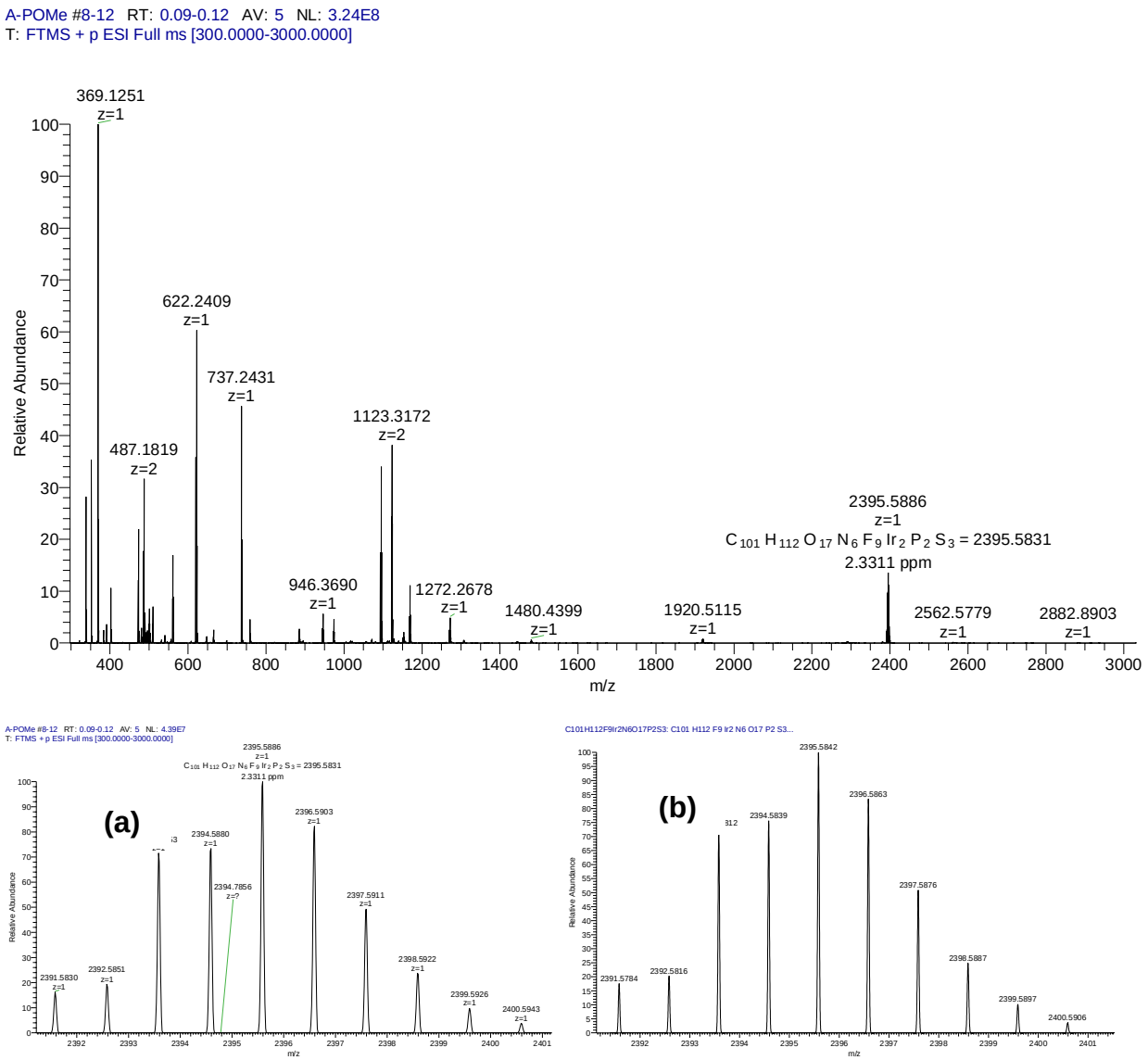

Figure S32. (Top) HRMS (ESI) spectrum of complex **A-POMe** (Bottom) Expanded peak at m/z = 2396 (a) and theoretical isotope pattern of $[M - OTf^-]^+$ (b).

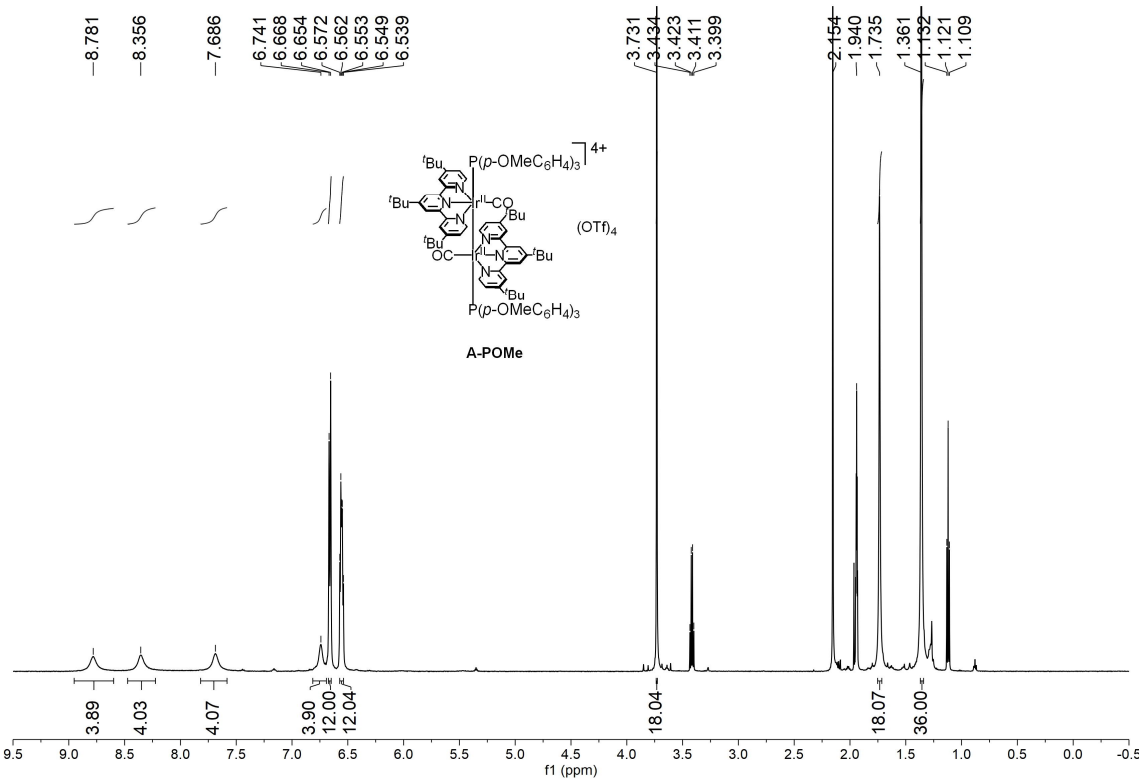

Figure S33. ^{1}H NMR spectrum of complex **A-POMe** in CD_3CN.

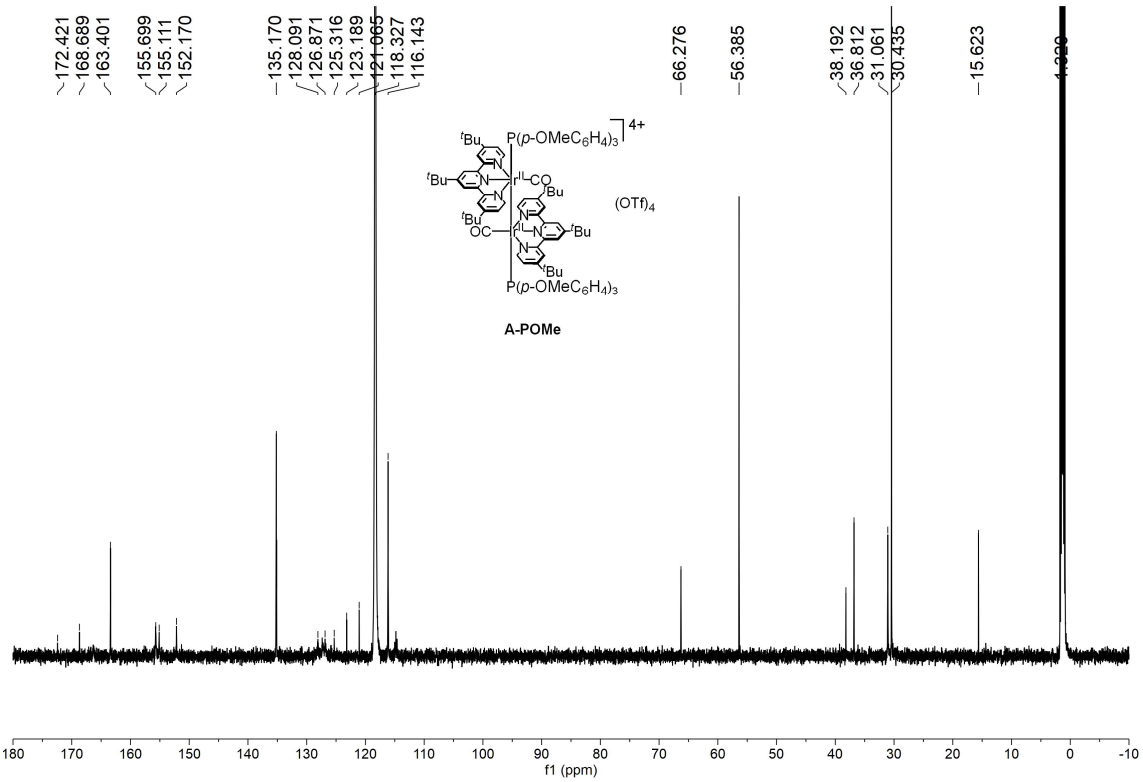

Figure S34. ^{13}C NMR spectrum of complex **A-POMe** in CD_3CN.

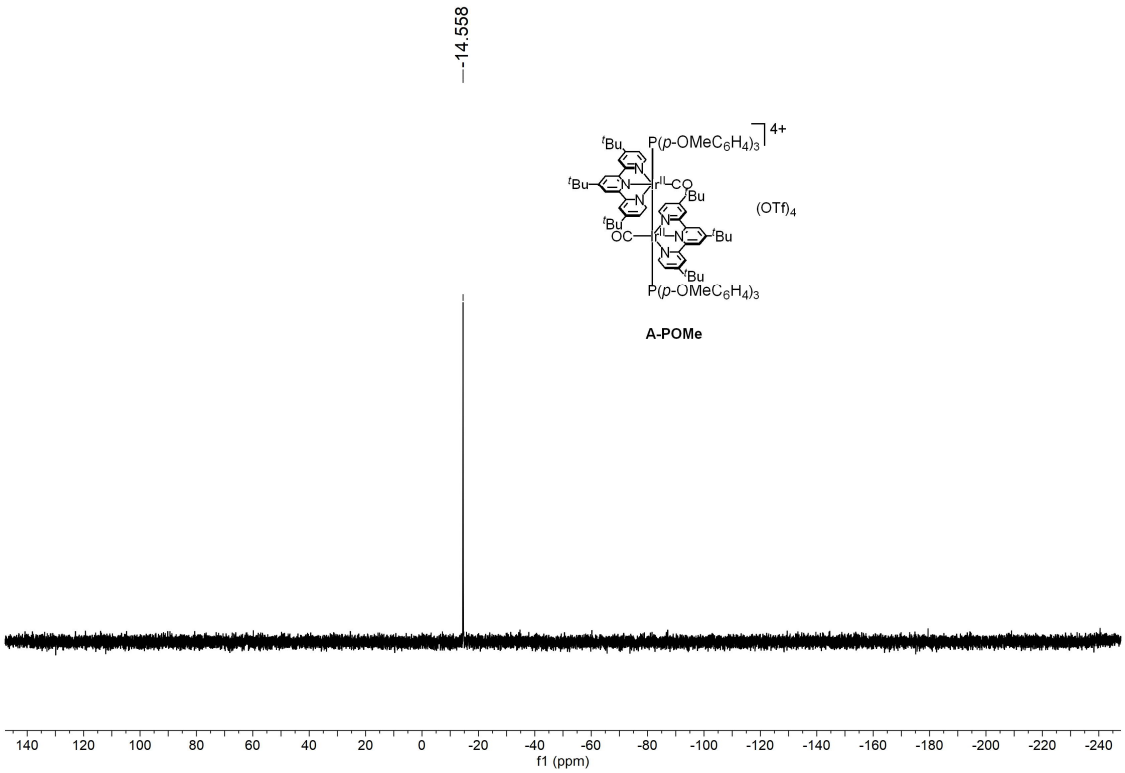

Figure S35. ^{31}P NMR spectrum of complex **A-POMe** in CD_3CN.

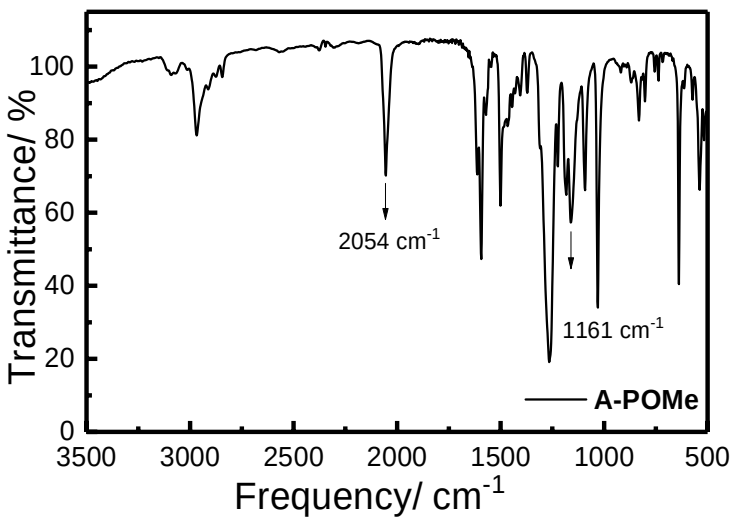

Figure S36. IR spectrum of complex **A-POMe** in KBr showing ν(C≡O) and ν(S=O) stretching.

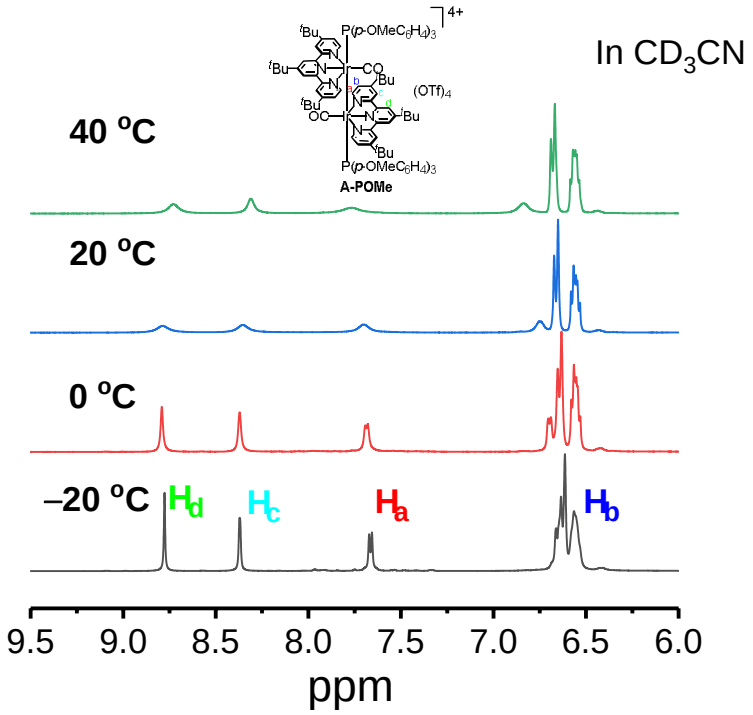

Figure S37. Variable-temperature ^{1}H NMR spectra of complex **A-POMe** in CD_3CN.

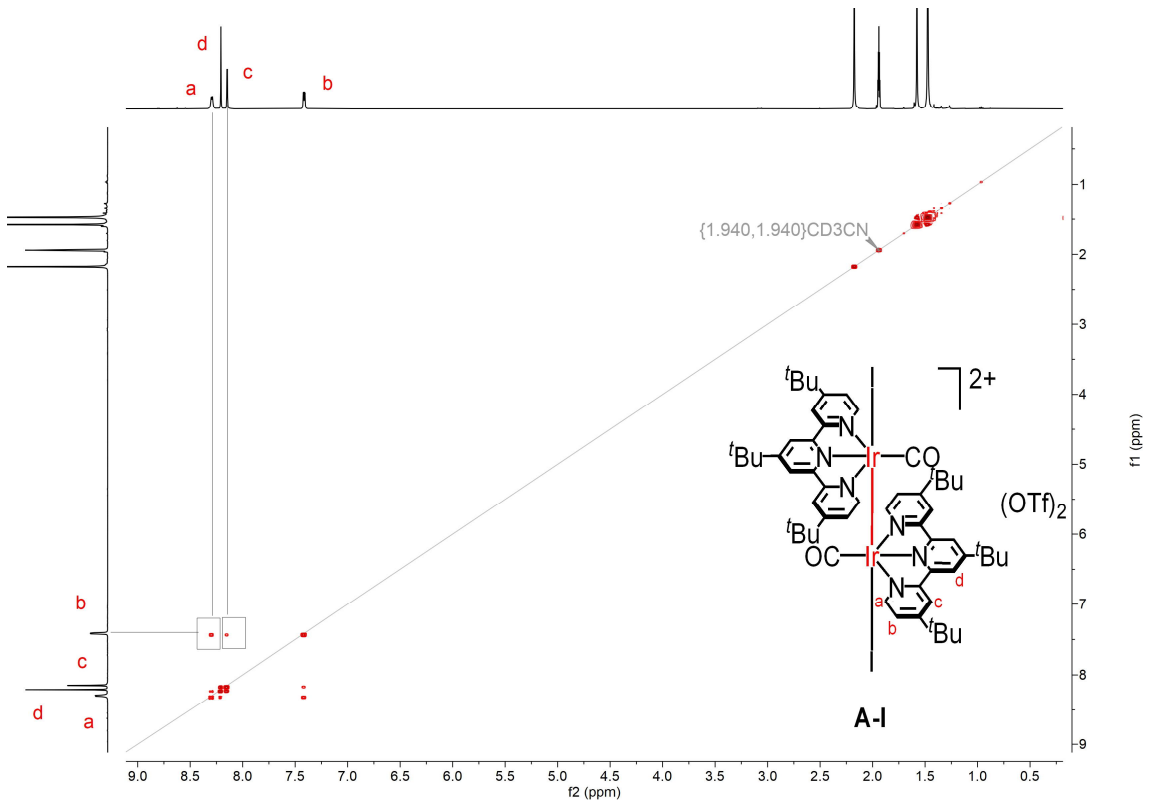

Figure S38. COSY spectra of complex **A-I** in CD_3CN.

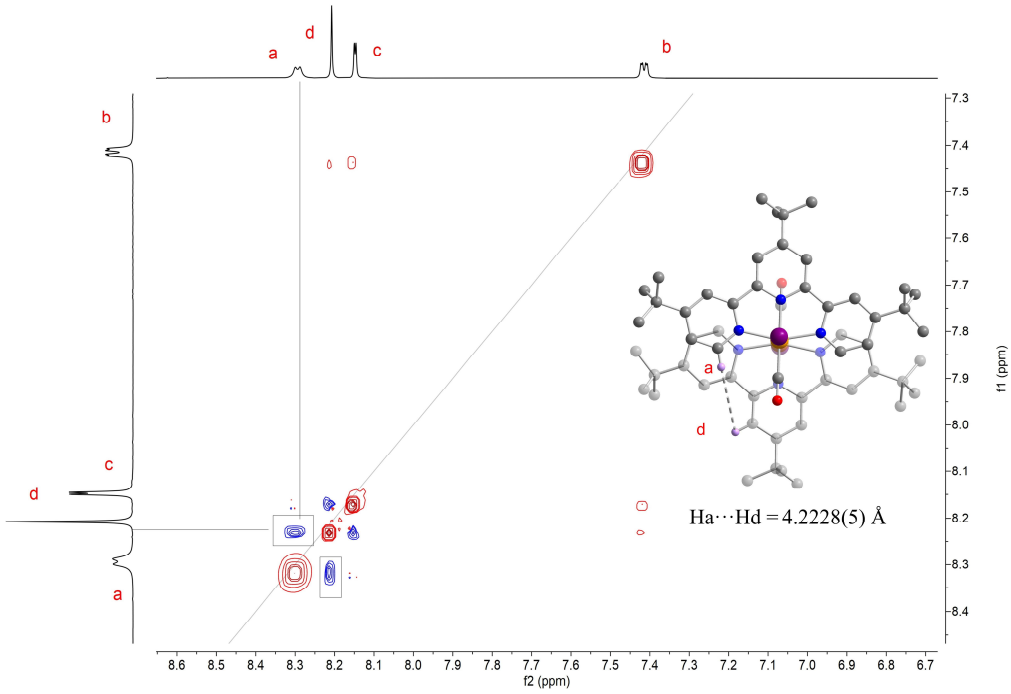

Figure S39. NOESY spectra of complex **A-I** in CD_3CN at room temperature.

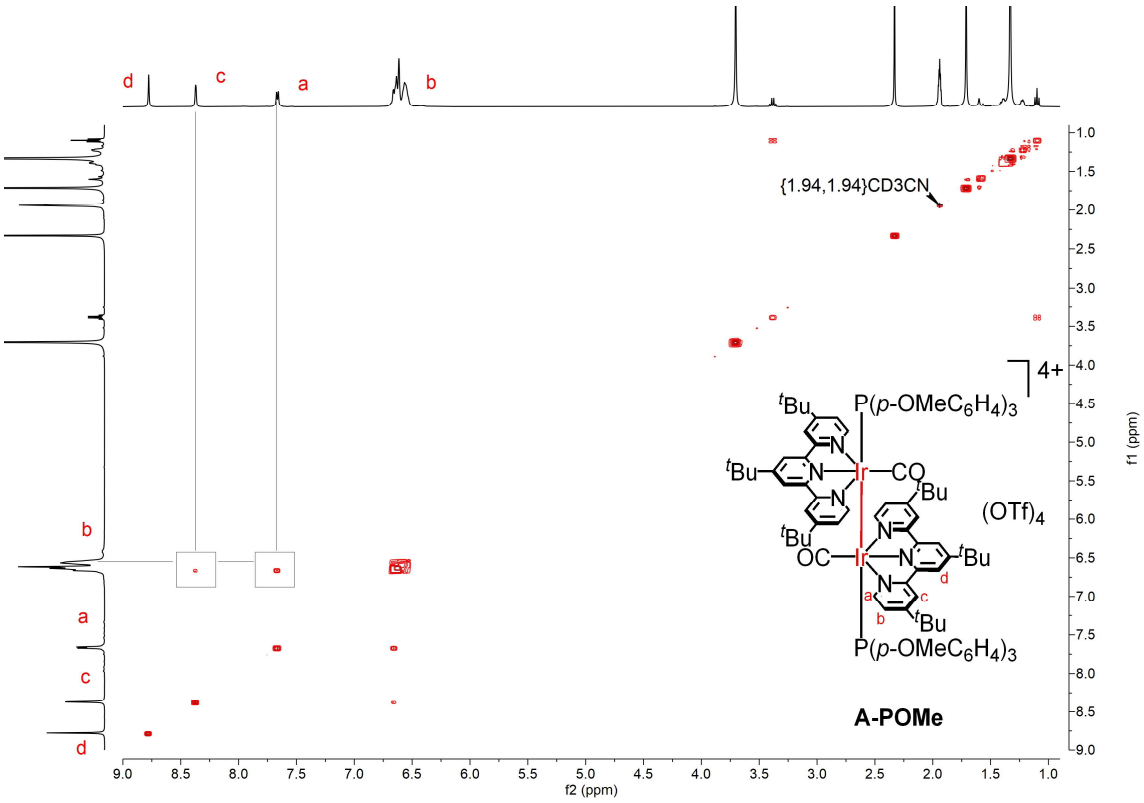

Figure S40. COSY spectra of complex **A-POMe** in CD_3CN at -20°C.

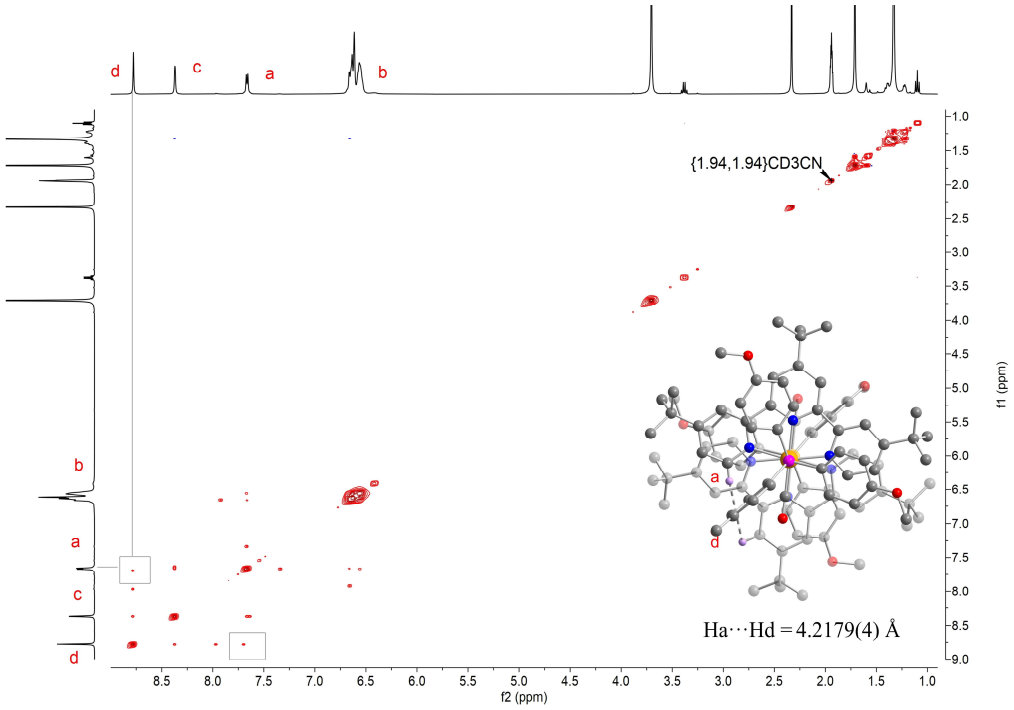

Figure S41. NOESY spectra of complex **A-POMe** in CD_3CN at -20ºC.

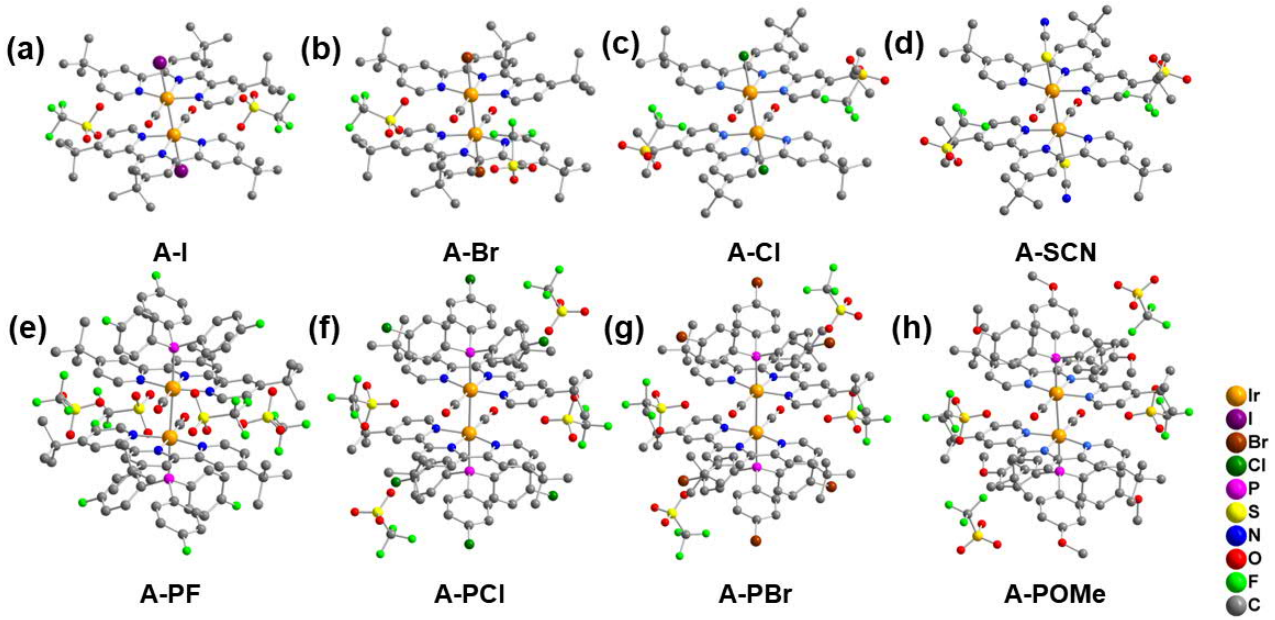

Figure S42. Perspective drawing of **A-I**, **A-Br**, **A-Cl**, **A-SCN**, **A-PF**, **A-PCl**, **A-PBr** and **A-POMe** (**a-h**) showing the position of their counter anions.

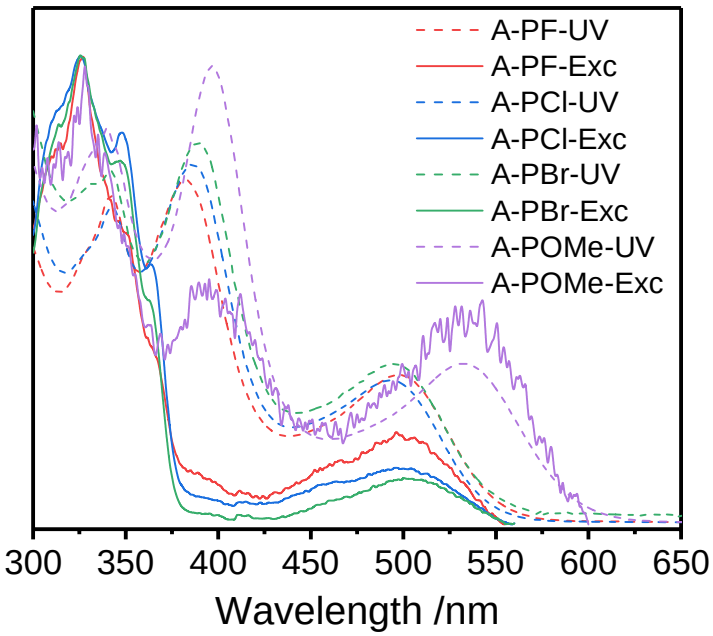

Figure S43. Normalized excitation spectra and UV-Vis absoprion spectra of **A-PF**, **A-PCl**, **A-PBr** and **A-POMe** in CH_3CN solution at 298 K. Emission intensity monitored at 680 nm for **A-PF**, 680 nm for **A-PCl**, 680 nm for **A-PBr** and 750 nm for **A-POMe**.

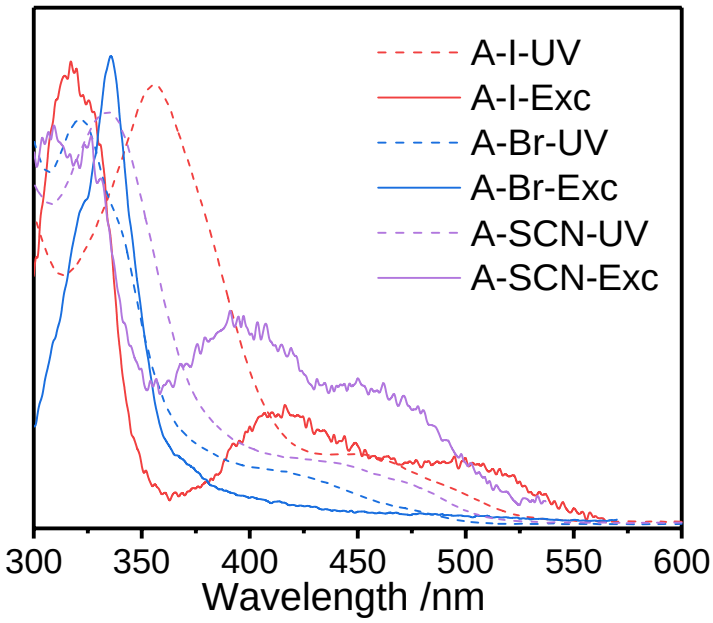

Figure S44. Normalized excitation spectra and UV-Vis absoprion spectra of of **A-I**, **A-Br** and **A-SCN** in CH_3CN solution at 298 K. Emission intensity monitored at 700 nm for **A-I**, 700 nm for **A-Br** and 650 nm for **A-SCN**.

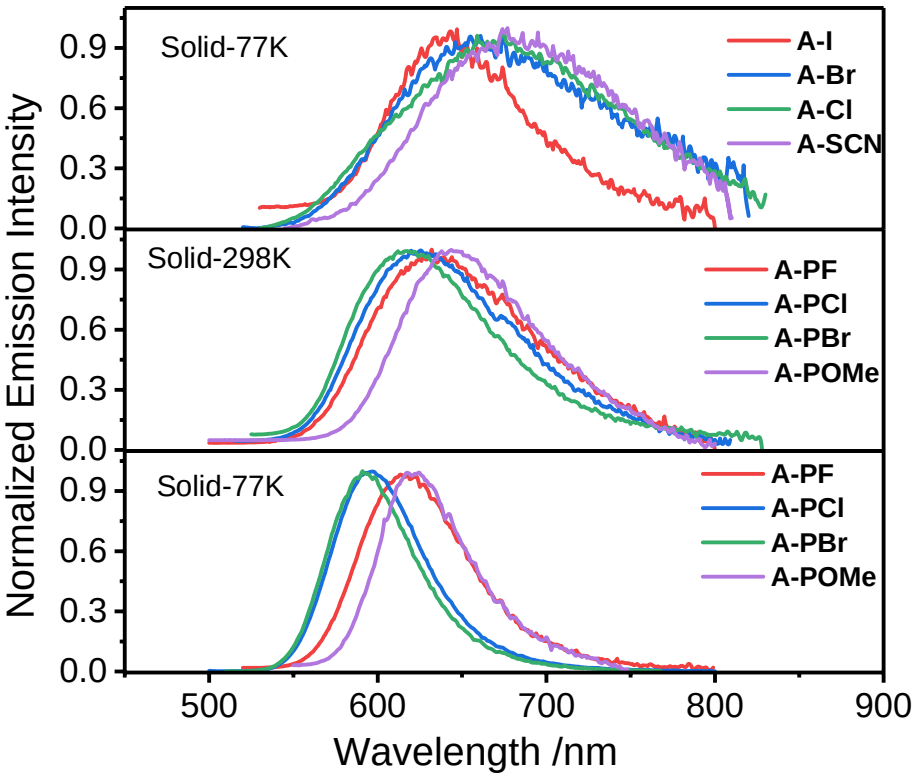

Figure S45. Luminescence spectra of diiridium(II) complexes from the anion series in solid state at 77K, and the P series in solid state at both 298 K and 77 K.

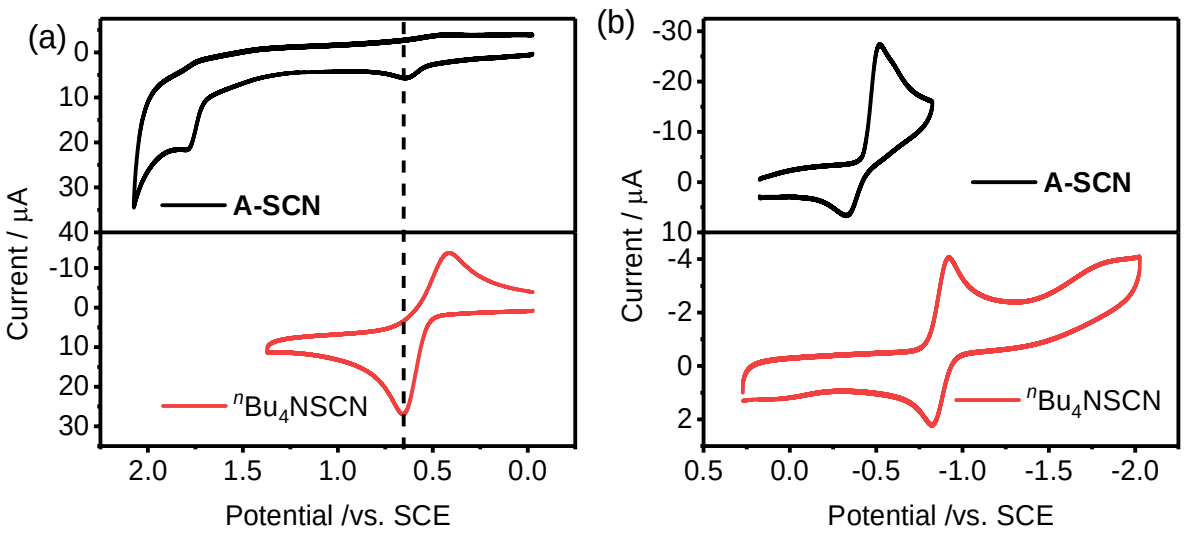

Figure S46. Cyclic voltammograms for oxidative (a) and reductive (b) scans of **A-SCN** and $^{n}Bu_4NSCN$ in CH_3CN solution (0.1 M $^{n}Bu_4NPF_6$) at 298 K. Scan rate = 100 mV/s.

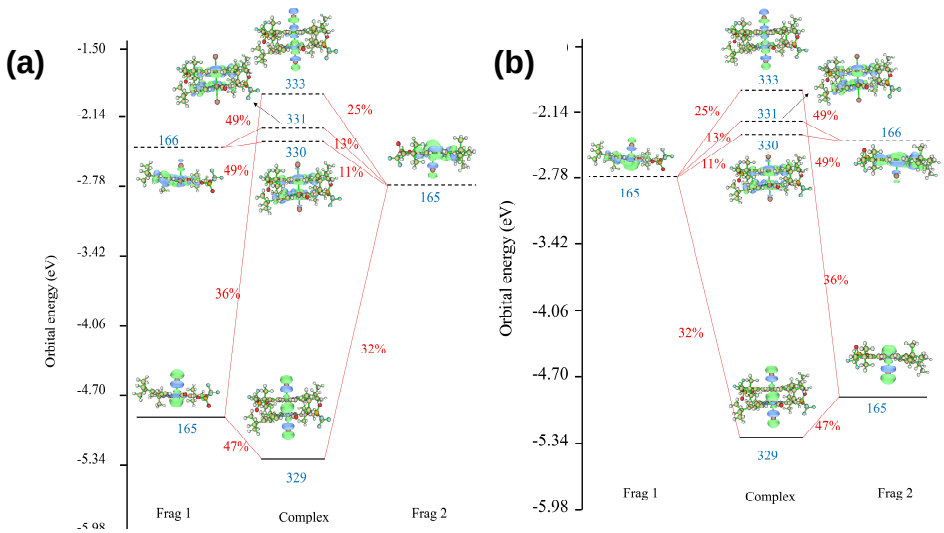

Figure S47. Orbital interaction diagrams of complex **A-I** (a) α orbitals (b) β orbitals by SMD B3LYP //B3LYP method.

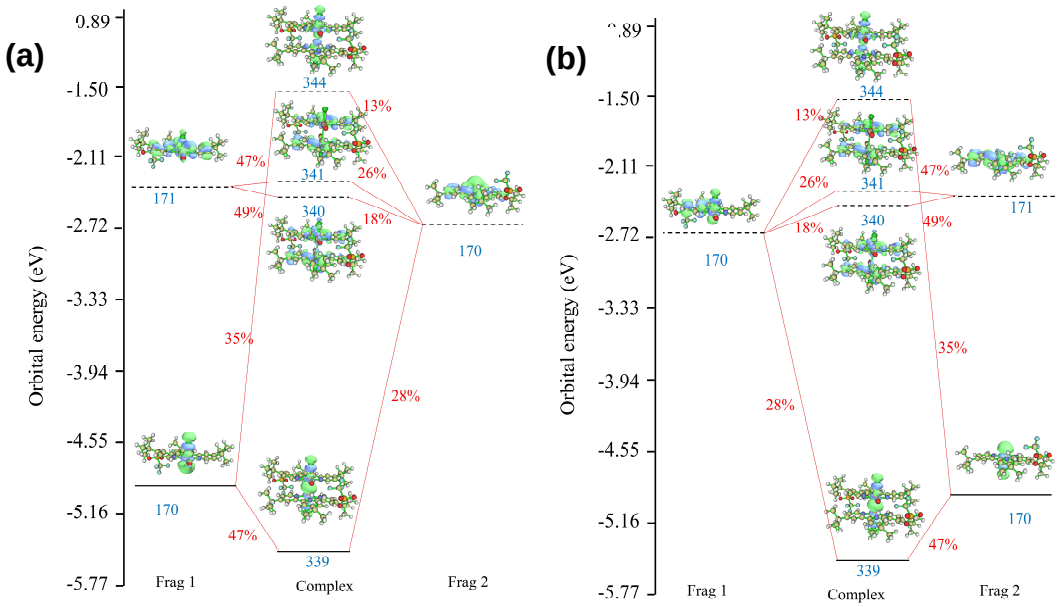

Figure S48. Orbital interaction diagrams of complex **A-Cl** (a) α orbitals (b) β orbitals by SMD B3LYP //B3LYP method.

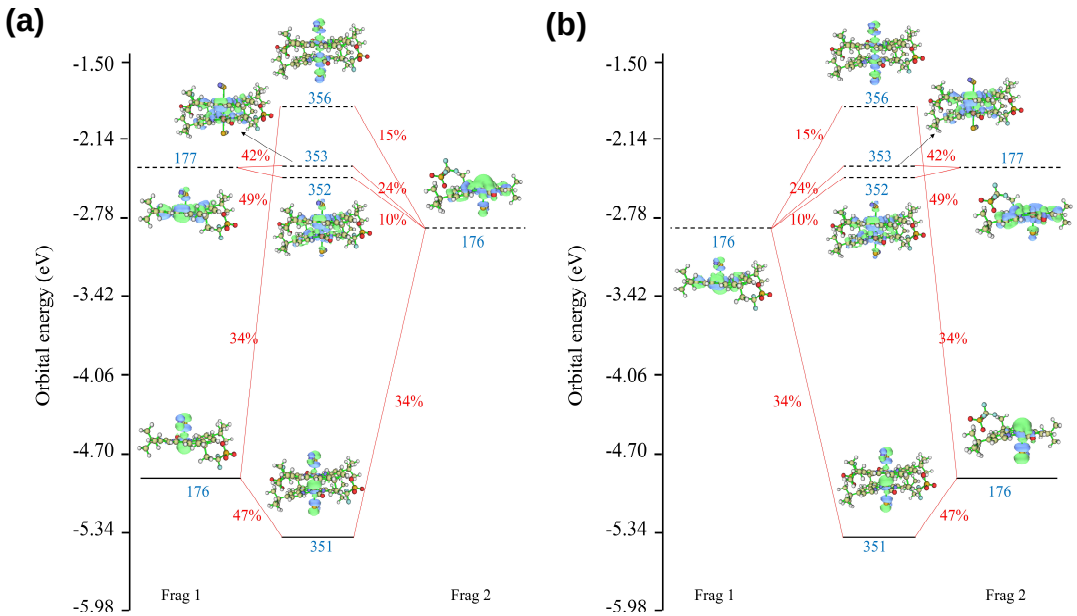

Figure S49. Orbital interaction diagrams of complex **A-SCN** (a) α orbitals (b) β orbitals by SMD B3LYP //B3LYP method.

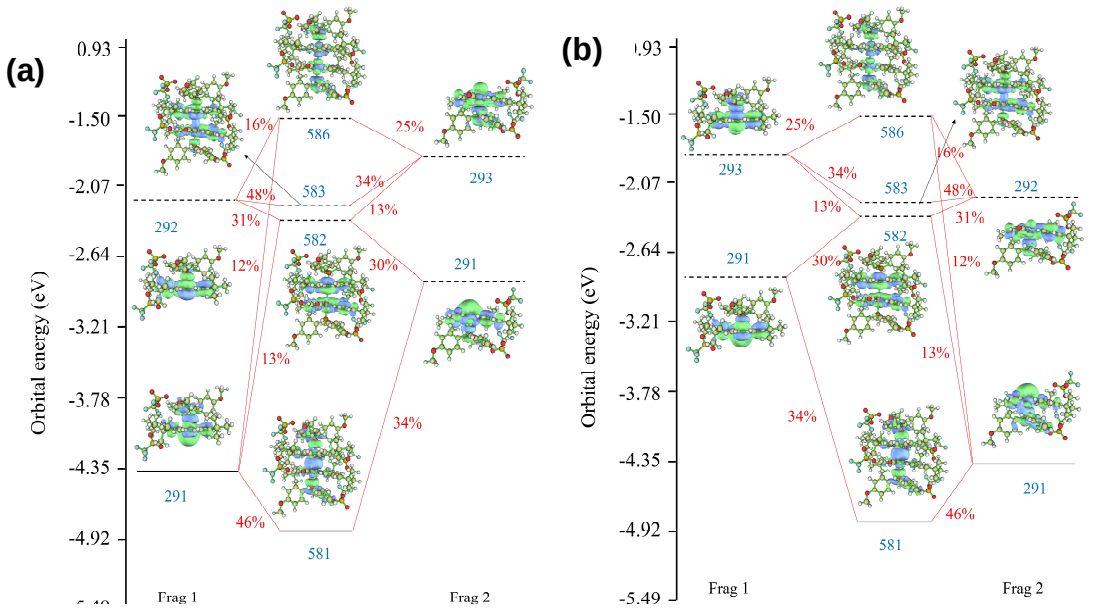

Figure S50. Orbital interaction diagrams of complex **A-POMe** (a) α orbitals (b) β orbitals by SMD B3LYP //B3LYP method.

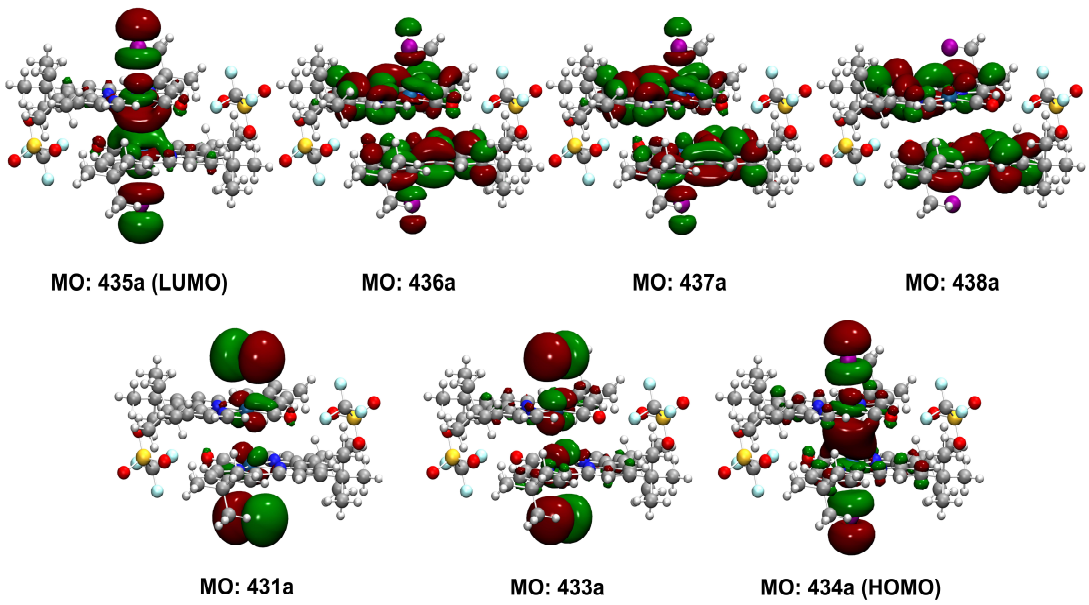

Figure S51. The corresponding absorption orbitals of complex **A-I** in acetonitrile solvent by the CPCM TD B3LYP-D//B3LYP-D3BJ method based on the B3LYP-D3BJ optimized geometries using ORCA 6.0.0.

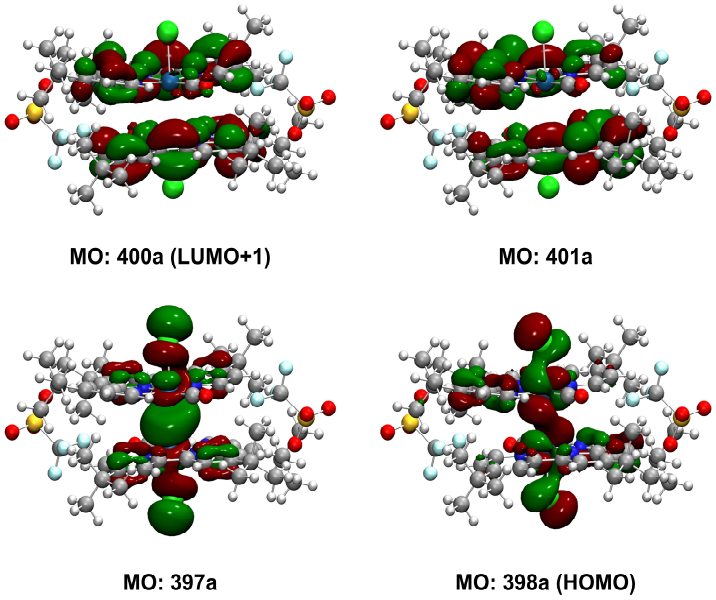

Figure S52. The corresponding absorption orbitals of complex **A-Cl** in acetonitrile solvent by the CPCM TD B3LYP-D3//B3LYP-D3BJ method based on the B3LYP-D3BJ optimized geometries using ORCA 6.0.0.

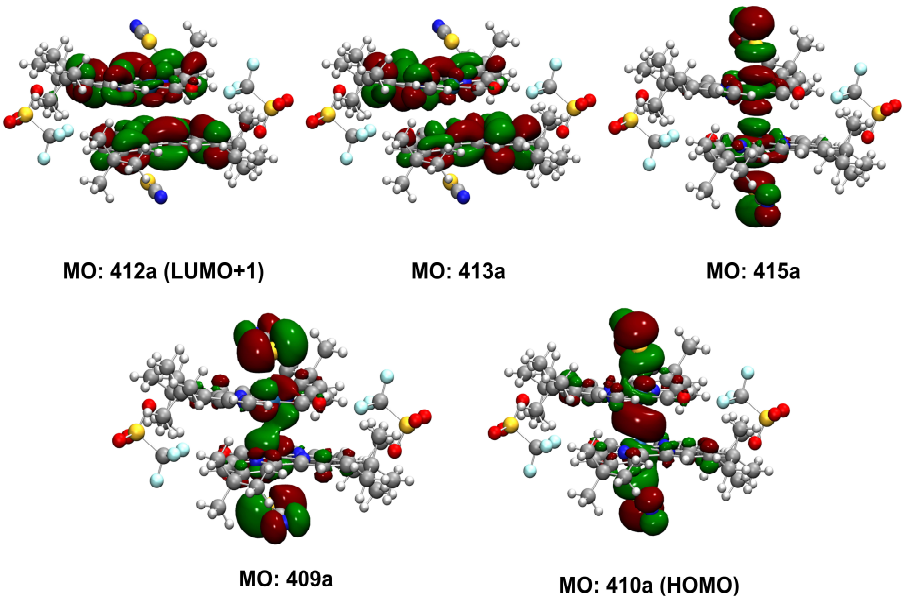

Figure S53. The corresponding absorption orbitals of complex **A-SCN** in acetonitrile solvent by the CPCM TD B3LYP-D3//B3LYP-D3BJ method based on the B3LYP-D3BJ optimized geometries using ORCA 6.0.0.

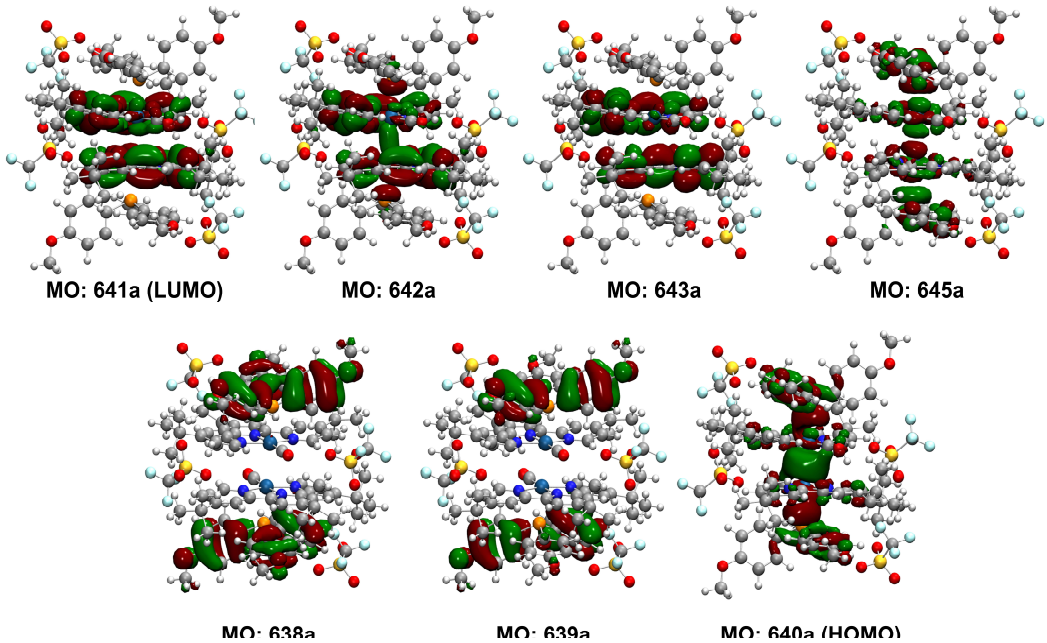

Figure S54. The corresponding absorption orbitals of complex **A-POMe** in acetonitrile solvent by the CPCM TD B3LYP-D//B3LYP-D3BJ method based on the B3LYP-D3BJ optimized geometries using ORCA 6.0.0.

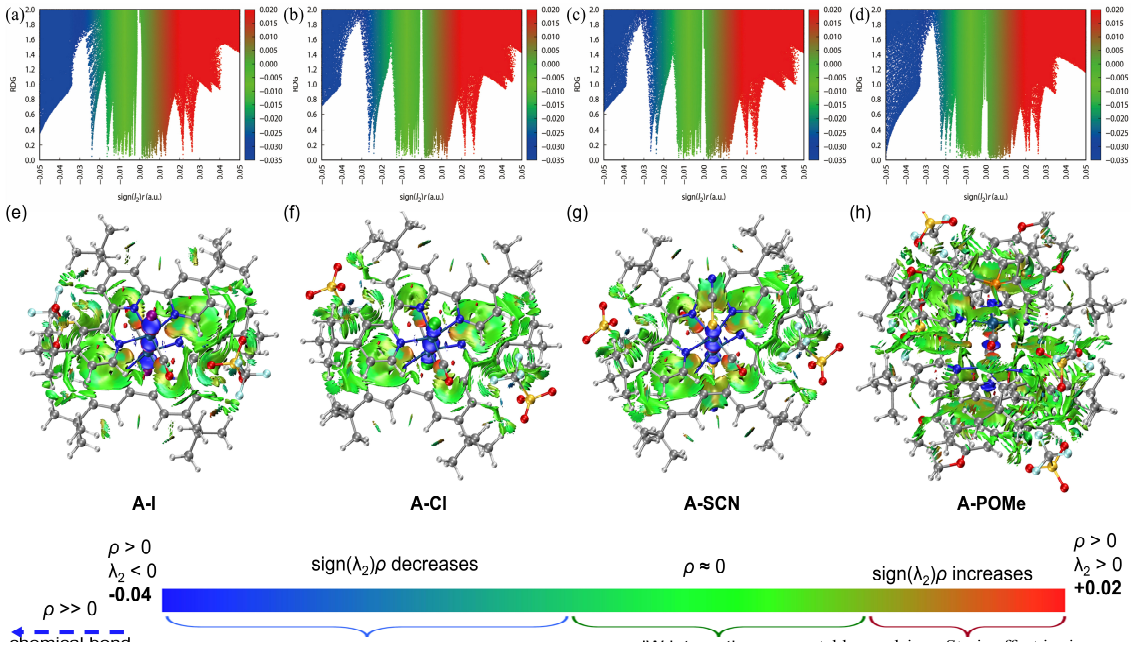

Figure S55. Scatter diagrams of **A-I** (a), **A-Cl** (b), **A-SCN** (c) and **A-POMe** (d); coloring contour surface diagrams in the dimer of **A-I** (e), **A-Cl** (f), **A-SCN** (g) and **A-POMe** (h).

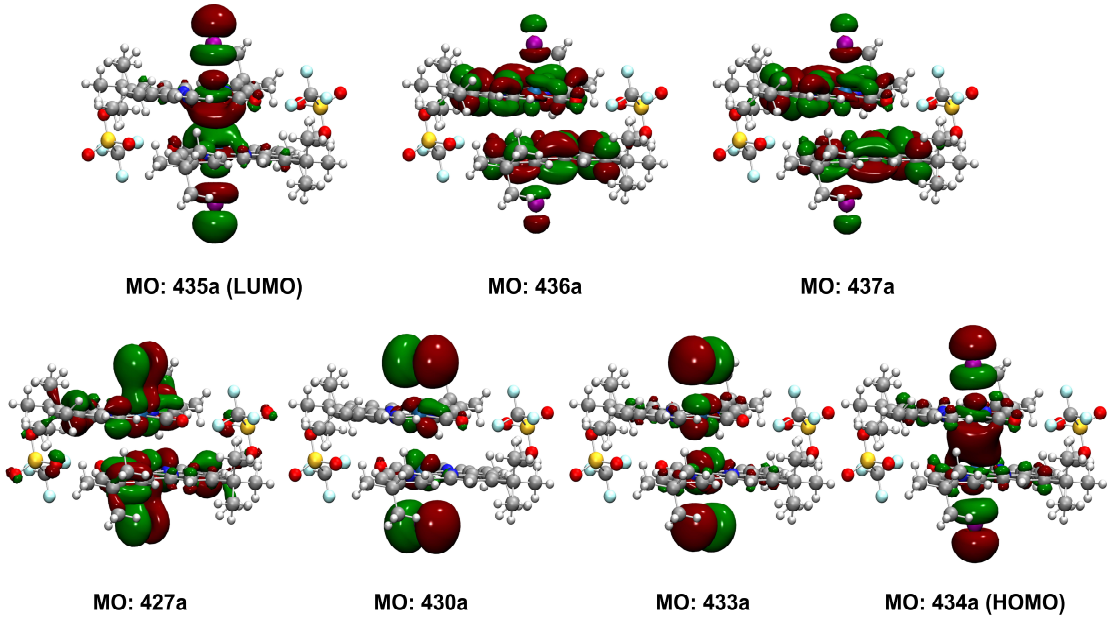

Figure S56. The corresponding emission orbitals of triplet **A-I** in acetonitrile solvent by the CPCM TD B3LYP-D3//B3LYP-D3BJ method based on the B3LYP-D3BJ optimized geometries using ORCA 6.0.0.

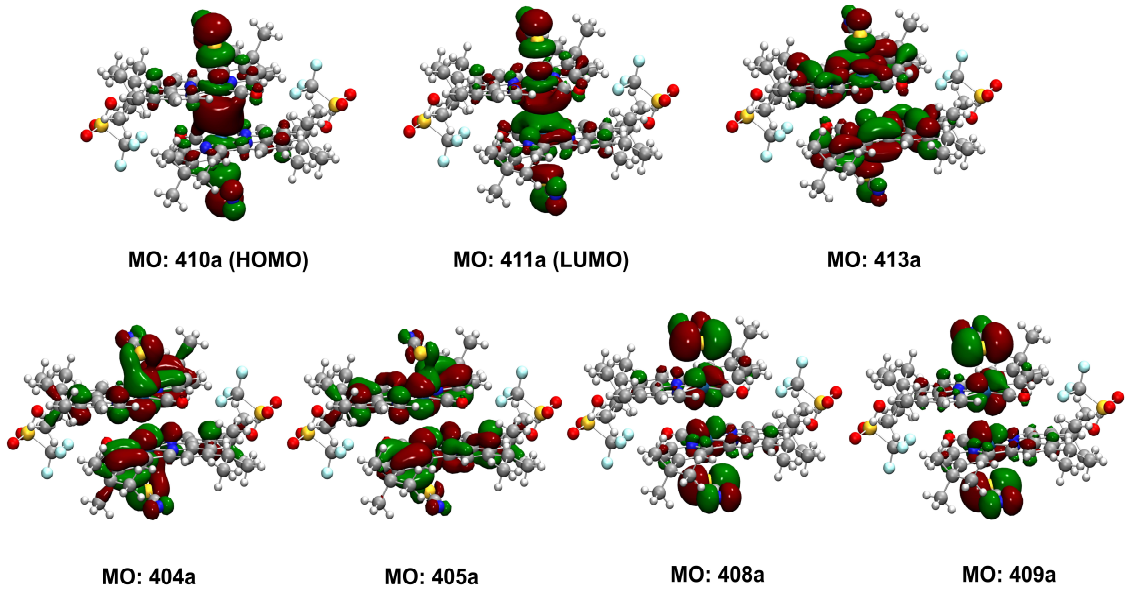

Figure S57. The corresponding emission orbitals of triplet **A-SCN** in acetonitrile solvent by the CPCM TD B3LYP-D3//B3LYP-D3BJ method based on the B3LYP-D3BJ optimized geometries using ORCA 6.0.0.

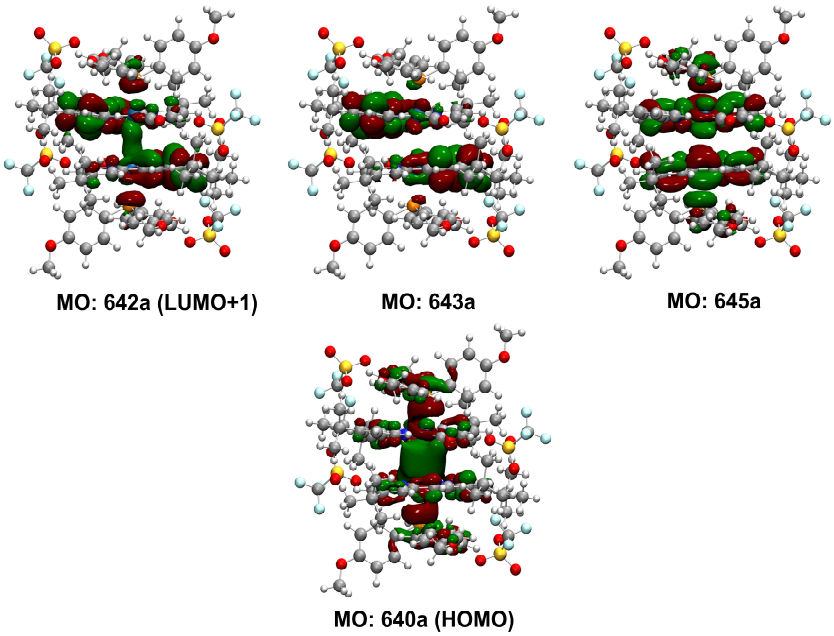

Figure S58. The corresponding emission orbitals of triplet **A-POMe** in acetonitrile solvent by the CPCM TD B3LYP-D//B3LYP-D3BJ method based on the B3LYP-D3BJ optimized geometries using ORCA 6.0.0.